



Research papers

Coastal upwelling over the North Aegean Sea: Observations and simulations

Yannis S. Androulidakis^{a,b,*}, Yannis N. Krestenitis^b, Stella Psarra^c^a Rosenstiel School of Marine and Atmospheric Science, RSMAS/MPO, University of Miami, 4600 Rickenbacker Cswy., Miami, FL 33149, USA^b Laboratory of Maritime Engineering and Maritime Works, Aristotle University of Thessaloniki, Greece^c Institute of Marine Biology of Crete, Hellenic Centre of Marine Research, Heraklion, Crete, Greece

ARTICLE INFO

Keywords:

North Aegean
Upwelling
Black Sea waters
Numerical simulations

ABSTRACT

Prevailing northerly winds influence the eastern coastal area of the North Aegean (N. Aegean) Sea and form a strong front due to occurring upwelling waters during the summer months. The upwelling processes over the Lesvos coastal region are investigated with the use of *in situ* measurements, numerical simulations, and satellite observations. The interaction of the major lateral buoyant input of Black Sea Waters (BSW) with the upwelling processes and waters is also investigated. The offshore propagation of the up-welled waters over the central N. Aegean region and their interactions with the permanent central cyclonic eddies, the major BSW patterns and the general Aegean cyclonic circulation determine their fate over the Aegean Sea. The upwelling depth is small over the Lesvos coastal region and is restricted in the subsurface ocean (< 40 m). The shallow upwelling depth is also confirmed by the reduction of the Apparent Oxygen Utilization (AOU) levels during upwelling events while the pre-existing surface waters, affected by the BSW plume reveal higher AOU values. More importantly, the up-welled waters come from above the thermocline nutrient depleted layer and, therefore, no major blooming events may be triggered in the central and eastern Aegean during the summer months. Southerly winds on the other hand, have a double effect. They form upwelling unfavorable conditions and they may facilitate the BSW propagation towards the upwelling region, blocking the eastward Ekman current and strengthening the stratification due to the formation of a surface barrier layer.

1. Introduction

The hydrodynamic and physical characteristics of the North Aegean (N. Aegean) Sea, especially over the upper-ocean, are largely determined by the dominant meteorological conditions (Poulos et al., 1997) in tandem with buoyancy-driven currents induced by the inflow of low-salinity Waters of Black Sea origin (BSW) through the Dardanelles Straits (Zervakis and Georgopoulos, 2002; Kourafalou and Barbopoulos, 2003; Androulidakis et al., 2012b). The SST (Sea Surface Temperature) seasonal mean patterns reveal strong cooling that is associated with upwelling phenomena under northerly summer winds along the eastern boundary of the basin (Albanakis, 1999; Kourafalou and Barbopoulos, 2003; Skliris et al., 2010) and especially over the coastal areas, south of the Dardanelles Straits (Zervoudaki et al., 1999), such as the coastal region of western Lesvos (Fig. 1). Recurring upwelling in the eastern Aegean Sea was first studied by Ünlüata (1986).

The dominant winds during summer, blowing over the whole Aegean Sea, are characterized by strong magnitudes with northerly components (Valioulis and Krestenitis, 1994; Poulos et al., 1997).

There is a clear positive SST gradient from east to west, related to the upwelling favorable northerly winds (“Meltemia” or “Etesian Winds”, Kourafalou and Barbopoulos, 2003; Skliris et al., 2010). Generally, these winds are northeasterly over the N. Aegean, northerly over the Central Aegean and turn to northwesterly over the South Aegean (Savvidis et al., 2004). The related upwelling process along the eastern Aegean coastal and shelf areas falls under the generalized case of the continental shelf seawaters, where the wind blows parallel to the coast, with the coastline on the left side of the wind direction in the case of the northern hemisphere. Savvidis et al. (2004), based on simulation results, showed that in the case of the Etesians Winds, applied over the whole Aegean basin with wind speed of 10 m/s, upwelling processes start to develop during a period of a few days. The prevailing northerly winds form a strong front due to occurring upwelling waters over Saros Gulf, south of the Dardanelles Straits and, in the west of Lesvos and Chios islands (Sayın et al., 2011). According to Sayın et al. (2011), the up-welled waters may flow over a larger area offshore from Lesvos Island and up to Chios Basin, affecting the general circulation and forming two cyclonic eddies during summer over the broader east-central region.

* Corresponding author at: Laboratory of Maritime Engineering and Maritime Works, Aristotle University of Thessaloniki, Greece.

E-mail addresses: iandroul@civil.auth.gr (Y.S. Androulidakis), ynkrest@civil.auth.gr (Y.N. Krestenitis), spsarra@hcmr.gr (S. Psarra).

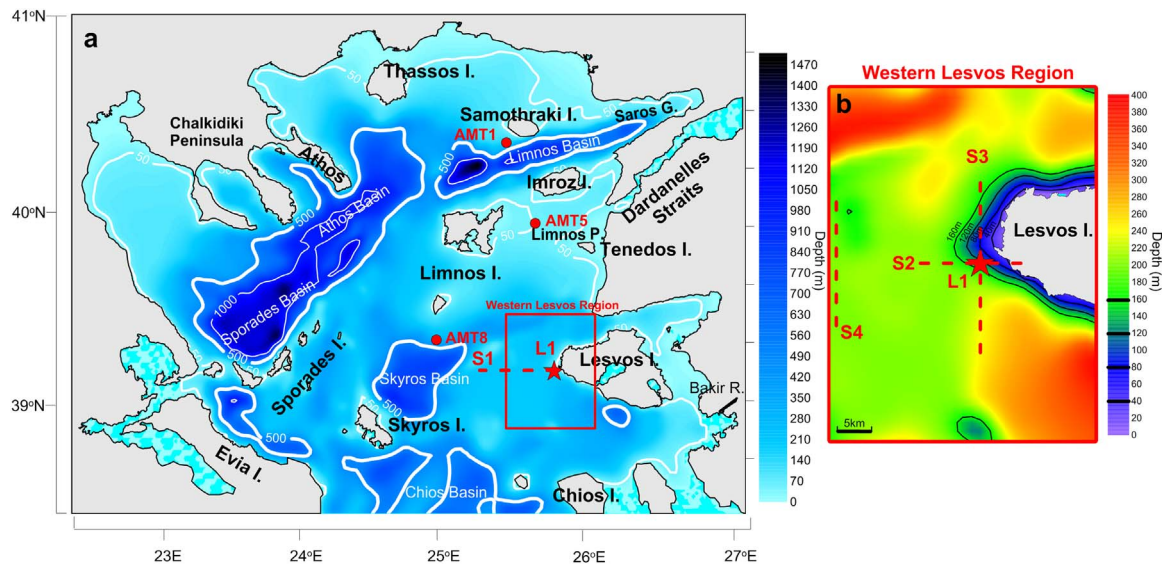


Fig. 1. Bathymetry maps (m) indicating (a) the main features (deep basins, islands and the Dardanelles Straits) of the N. Aegean Sea HYCOM model (NAS-HYCOM) domain and (b) the western Lesvos region. Left (western Aegean) land mass is the Greek mainland; right (eastern Aegean) land mass is the Asia Minor (Turkish) mainland. The solid lines mark the 20 m, 40 m, 50 m, 60 m, 80 m, 120 m, 160 m, 500 m and 1000 m isobaths. The red star indicates the L1 (Poseidon System Buoy) and the red circles indicate the R/V Aegeo October 2013 cruise stations (AMT1, AMT5, AMT8). Sections S1, S2, S3 and S4 are indicated with dashed red lines. (For interpretation of the references to color in this figure legend, the reader is referred to the web version of this article).

The BSW input is the most important buoyant input over the N. Aegean region, affecting the largest part of the upper-ocean, especially during spring and summer, when the discharge through the Dardanelles usually reveals its highest values (Ünlüata et al., 1990). However, recent simulations of the Dardanelles Straits outflow, based on Black Sea water balance (Androulidakis et al., 2012b), showed that strong discharges may also occur in other seasons, such as autumn and winter, due to alterations of river outflows and E-P variability of the Black Sea. Maderich et al. (2015), based on numerical simulations, showed that vertical mixing along the Turkish Strait System determines the flow characteristics of the upper layer towards the Aegean Sea, while the highest upper-layer transport in the Dardanelles exit may occur in spring. The BSW plume induces buoyancy-driven transport pathways that affect the basin-wide N. Aegean dynamics and may influence several Aegean physical dynamics, such as dense water formation (Zervakis et al., 2000; Androulidakis et al., 2012a), mixed layer characteristics and interactions with South Aegean water masses (Theocharis et al., 1999). In summer months, the strong northerly winds in combination with strong BSW discharge rates may bring brackish waters, originated from the Black Sea, directly to the Southwest, towards the Evia Island area (Androulidakis et al., 2012b). The Dardanelles discharge values and furthermore the BSW propagation over the Aegean, used in this study, are based on the simulations by Androulidakis et al. (2012b). Their parameterization of BSW outflow, based on the Black Sea water balance, improved the model performance during summer 2002 in comparison with the use of historical outflow values (their Figs. 6 and 7).

The upwelling waters, on the other hand, may influence the physical and biological characteristics of the near-shore and broader central area. Generally, the upwelling colder waters, enriched with nutrients, move to the surface and may enhance the biological activity, enriching the fish-productivity of the coastal waters (Millan-Nunez et al., 1982). The BSW plume also affects the biological features of N. Aegean basin, such as nutrients, chlorophyll (Kucuksezgin et al., 1995; Ignatiades et al., 2002; Lagaria et al., 2016) and mesozooplankton (Siokou-Frangou et al., 2009) concentrations. BSW through its uninterrupted supply of small quantities of nutrients plays an important role in pelagic production of the N. Aegean Sea (Siokou-Frangou et al., 2002; Souvermezoglou et al., 2014). However, the BSW input through the Dardanelles Straits is enriched in organic rather than inorganic matter

(Zeri et al., 2014). To the best of our knowledge, the relation between the upwelling processes over the eastern N. Aegean coastal region and the major BSW plume has not been investigated in the past.

The aim of this study is the investigation of the upwelling processes over the continental shelf of the western Lesvos region, which is one of the most important Aegean upwelling regions. Five upwelling events are detected during the significantly active summer months of 2002 due to long periods with persistent strong northerly winds. The spreading and the relation of the up-welled waters with the broader N. Aegean water masses are also investigated. The impact of the large lateral input from the Black Sea during the upwelling periods is examined. We will show that the major circulation patterns of this brackish water mass over the N. Aegean and especially over the upwelling regions play an important role on the formation and evolution of the upwelling phenomena. We will describe several additional aspects, such as the upwelling depth, the vertical structure of the upwelling area, the differences between the physical characteristics of the up-welled waters and pre-existent and/or surrounding masses, based on *in situ* observations, high resolution numerical simulations, and satellite data. The work is based on the combination of observations with numerical results, produced by the North Aegean Sea Hybrid Coordinate Ocean Model (NAS-HYCOM; Androulidakis and Kourafalou, 2011; Androulidakis et al., 2012a, 2012b).

Following the Introductory section (Section 1), Section 2 includes the methodology of the work, the description of observations and simulations and the evaluation of the NAS-HYCOM during the study period, focused on the upwelling Lesvos region. The detected upwelling events, the respective prevailing atmospheric conditions and the major BSW evolution patterns are presented in Section 3. The surface circulation features, the evolution of the Ekman transport, the vertical structure over the upwelling region and possible implications of upwelling with dissolved oxygen concentrations are discussed in Section 4. A summary of concluding remarks is presented in Section 5.

2. Methods and data

2.1. *In situ* measurements

The *in situ* measurements used in the study are derived from a buoy of the Poseidon System, implemented and maintained by the Hellenic

Center for Marine Research (HCMR; <http://poseidon.hcmr.gr/>; Nittis et al., 2002). We used 3-hourly measurements from the Lesvos Poseidon Buoy (121 m depth), located 5 km offshore over the western coastal region of Lesvos (L1, 39° 09′ 0.346 N - 25° 48′ 0.472 E; Fig. 1) for the summer of 2002. The relatively large depth and distance from the coast of the buoy ensure that the measured parameters and especially the upper-ocean currents are not topographically stirred by the nearby coast and local bottom topography. The observed data used in this study include SST and Sea Surface Salinity (SSS) measurements in 1 m depth in order to investigate the evolution of the surface mass characteristics under upwelling and non-upwelling conditions. Additional available temperature measurements in 10 m, 20 m, 30 m and 40 m were also collected from L1 Poseidon Buoy in order to investigate the vertical profile of the upwelling region. Moreover, the available temperature and surface salinity observations are also used to evaluate the performance of the numerical simulations, especially over the study upwelling region (see Sections 2.3.2 and 3.3), while Dissolved Oxygen (DO) surface measurements (1 m), obtained at the L1 Buoy, are also used to examine the upwelling over the study area and the differences between the up-welled waters and the pre-existing surface masses (see Section 4.3). Wind data (magnitude and direction) were derived from the L1 Buoy in order to examine the atmospheric conditions during summer of 2002. Additional CTD measurements of DO, temperature and salinity were also collected during the R/V Aegeao (HCMR) cruise in October 2013, conducted in the framework of the project THALES: “Technological and oceanographic cooperation network for the study of mechanisms fertilizing the North-East Aegean Sea” (<http://thales-aegeanmartech.hcmr.g>), in order to investigate the two-layer structure due to the intrusion and spreading of the BSW plume into the N. Aegean Sea; the cruise’s stations (Fig. 1a), used in the study, are located in the proximity of the Dardanelles Straits (AM5), along the northwestern BSW pathway (AM1) and over the central N. Aegean close to Lesvos Island (AM8).

2.2. Satellite imagery

Satellite data, covering the study region and period, were collected from two sources. The first source is the Copernicus Marine Environment Monitoring Service (<http://marine.copernicus.eu/>) that provides horizontal distributions of chlorophyll-a (chl-a) concentrations from multi-satellite sources. The Mediterranean surface chl-a fields have daily time-step and 4 km spatial resolution. The final product is derived by data, collected by the merging of SeaWiFS, MODIS-Aqua and MERIS sensors, and it is mainly used to investigate the BSW circulation patterns over the N. Aegean region (see Section 3.3).

The second source of satellite data is the Group for High Resolution SST (GHRSSST; <https://www.ghrsst.org/>) that includes gridded surface temperature fields. SST variability is an important oceanic indicator in upwelling dynamics. The GHRSSST data (Donlon et al., 2009) are collected from the Multi-sensor Ultra-high Resolution (MUR) analysis project, which produced Level 4 SST fields with 1–2 km horizontal resolution (1/90°×1/90°) and daily interval. The horizontal scale of the collected fields covers the entire N. Aegean domain, and the data are used to detect the upwelling events over the eastern N. Aegean Sea and to evaluate the performance of the simulations with respect to the surface temperature (See Section 3.3).

2.3. Numerical simulations

2.3.1. Model description

The implementation of Hybrid Coordinate Ocean Model (HYCOM, <http://hycom.org>; Chassignet et al., 2007) in the N. Aegean Sea is the NAS-HYCOM model, which extends from 22.5°E to 27.1°E and from 38.4°N to 41.0°N (Fig. 1a). The horizontal resolution of NAS-HYCOM

is 1/50° x 1/50° (~2.2 km). Certain shallow passages near the model nesting boundary are closed (Fig. 1a), as they are not important for the purposes of this study and to avoid topographic mismatching with the coarser outer model (initial and boundary conditions). The hybrid vertical coordinate structure of HYCOM is a very appropriate operation in investigating the upwelling processes over the continental shelves of the complex N. Aegean environment (topography and lateral inputs) and in simulating the vertical structure variability due to buoyant plume spreading over the surface layers (e.g. BSW). The transformation of the vertical hybrid coordinates (20 in the case of NAS-HYCOM) between isopycnal, sigma and cartesian (Bleck, 2002; Halliwell, 2004), is a significant advantage in such regions. Simulation results produced by NAS-HYCOM from April 2002 to December 2003, focusing over the summer of 2002, are used to describe the upwelling processes and support the observational findings.

The atmospheric forcing used in the NAS-HYCOM simulations is provided by the Poseidon Weather Forecasting System (<http://poseidon.hcmr.gr>) that has been developed in the framework of the POSEIDON-I project (Papadopoulos et al., 2002). The system is operational since October 1999 and provided 72-h forecasts in 1/10°×1/10° spatial resolution for the entire simulation period (2002–2003). Its central component is the SKIRON/Eta model (Kallos et al., 1997), which is a modified version of the Eta/NCEP model. The initial fields (01/04/2002) and the boundary conditions with the South Aegean are provided by the coarser (1/25°) data assimilated MEDiterranean-HYCOM (MED-HYCOM, Naval Research Laboratory, Stennis Space Center). MED-HYCOM was a part of the operational global HYCOM system (<http://hycom.org>). A two-layer Dardanelles flow parameterization, described in detail by Androulidakis et al. (2012b), is used in the simulations of summer 2002. More information about the model (HYCOM) and its N. Aegean implementation (NAS-HYCOM) were presented by Androulidakis and Kourafalou, (2011) and Androulidakis et al. (2012a, 2012b).

2.3.2. NAS-HYCOM validation during upwelling season

Extensive evaluation of the 2002–2003 simulation (including the summer study months of 2002) with NAS-HYCOM, using the Dardanelles flow parameterization based on the Black Sea water balance, was presented by Androulidakis et al. (2012b). They showed that this parameterization approach reveals higher correlation between model results (salinity and temperature) and satellite or *in situ* data, in comparison to previous parameterizations that employed climatologically or historically varying inputs through the Dardanelles Straits. Herein, we add an evaluation of the model, focusing on the Lesvos coastal region during summer 2002. Additional qualitative comparisons with satellite fields and *in situ* time series during the upwelling events are presented in Section 3.3.

Observational temperature values at several depths (L1 Poseidon Buoy) are compared with respective simulated values to evaluate the performance of the model in the water column of the upwelling region of Lesvos (Fig. 2). The linear fit between the surface measurements and model results is very close to the $y=x$ equation, supporting the good performance of NAS-HYCOM. Although the model slightly overestimates the temperature values at all depths, the mean Root Mean Squared Error (RMSE) over the upper water column (0–40 m) is less than 1 °C on average (RMSE=0.97; Table 1). The wide spreading of the values due to the summer temperature variations and the upwelling processes is apparent at both surface and 10 m depth, where both simulated and measured data range between 20 and 27 °C. The range shrinks at deeper layers and reaches its lowest values at 40 m depth (17–20 °C), which is usually out of the range of the summer vertical mixing (see Section 4.1). The best correlation between the two time series is observed for masses with lower temperature at all depths, while the bias is larger for higher temperature values (Fig. 2). The low temperature levels (< 22 °C) at upper layers (especially at 10 m) during July and August, when the upwelling study events took place (see

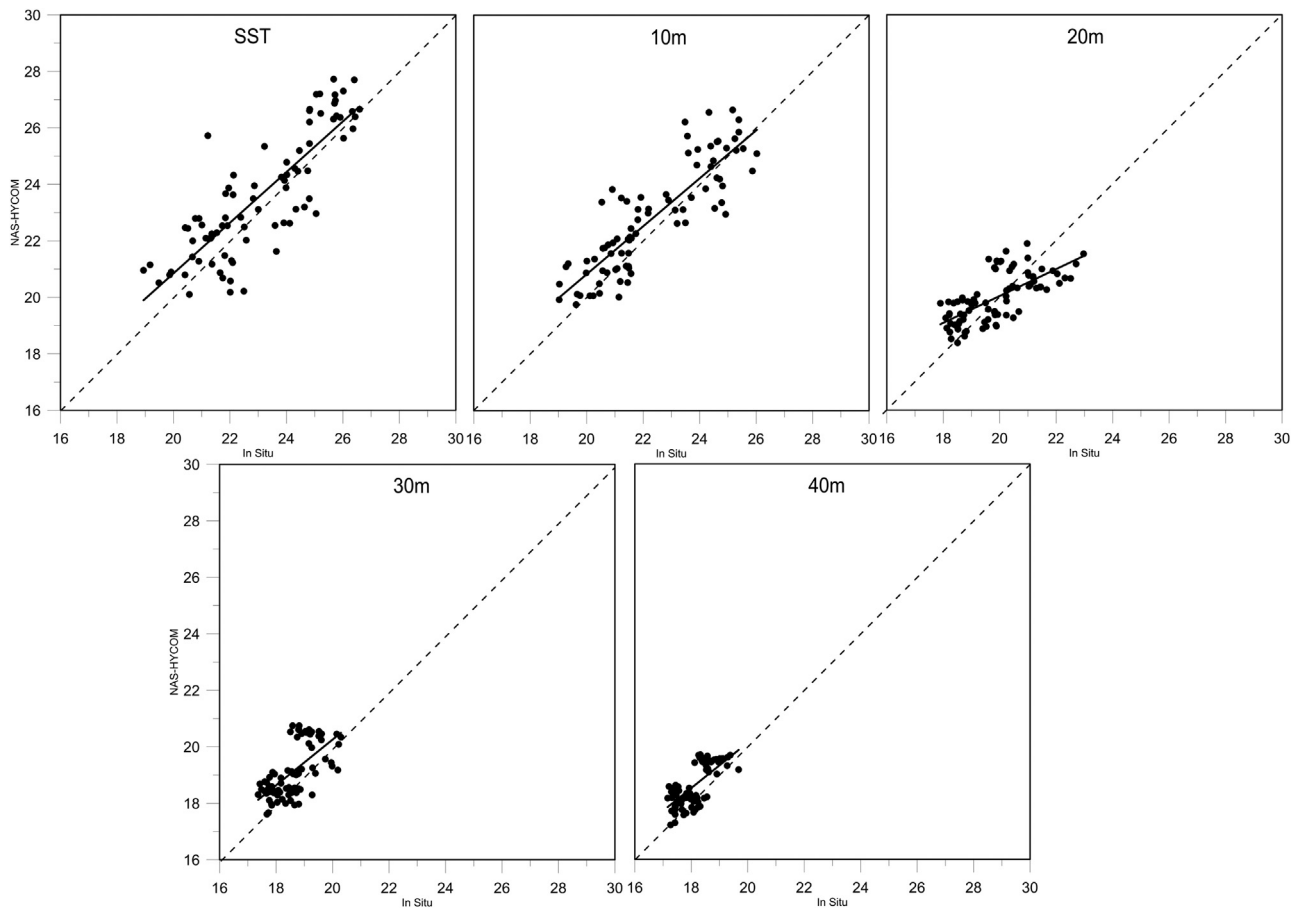


Fig. 2. Scatter comparison between daily *in situ* (L1 Poseidon Buoy) and modeled (NAS-HYCOM) surface, 10 m, 20 m, 30 m and 40 m temperatures for summer 2002 (June–August). The linear fit between the two time series, and the $x=y$ fit for each depth is indicated with a solid and a dashed line, respectively. The mean for each time series (simulated: Y and observed: X) is also presented.

Table 1

Pearson Correlation coefficient (r), Root Mean Square Error ($RMSE$), and Willmott Skill Score (W_s) of the Sea Surface (SST), 10 m, 20 m, 30 m and 40 m temperature as derived from daily L1 Poseidon Buoy observations and NAS-HYCOM simulations from June to August 2002.

	$RMSE$ (°C)	W_s	r
SST	1.32	0.90	0.84
10 m	1.04	0.90	0.88
20 m	0.92	0.79	0.69
30 m	0.88	0.70	0.66
40 m	0.72	0.72	0.71
Mean	0.97	0.80	0.76

Section 3.2), are strongly related to the up-welled waters. Although the higher $RMSEs$ appear among the upper layers for the entire summer (all daily values), the Pearson correlation coefficients (Pearson, 1903) for both surface ($r=0.84$) and 10 m ($r=0.88$) are very close to 1 (Table 1). All correlation coefficients are higher than 0.65 and they are statistical significant (p-values < 0.00001), indicating the good description of the temperature variation by the model, in agreement with the quantitative comparisons presented by Androulidakis et al. (2012b), for the entire simulation period (2002–2003) and the broader model domain (N. Aegean). We also employed the Willmott Skill Score (W_s) (Willmott, 1981) for the summer 2002 time series, in order to further quantitatively examine the model's performance. The calculation of W_s (Eq. (2)) employs the Mean Square Error (MSE):

$$MSE = (\langle m \rangle - \langle o \rangle)^2 + (S_m - S_o)^2 + 2S_m S_o(1 - r_c) \quad (1)$$

$$W_s = 1 - \frac{MSE}{\langle (|m - \langle o \rangle| + |o - \langle o \rangle|)^2 \rangle} \quad (2)$$

where m and o are the time series of the modeled and observed variables respectively, and $\langle \rangle$ denotes the temporal mean; S_m and S_o are the respective standard deviations. Perfect performance of the model is achieved when W_s coefficient is close to 1. NAS-HYCOM revealed scores higher than 0.70 in all cases, while the depth-averaged W_s is 0.80 (Table 1). The score is significantly high especially over the surface layers, where colder waters may be advected during summer ($W_s=0.90$), indicating the ability of the model to describe the upwelling processes and simulate the upwelling masses that may reach the surface of the Lesvos coastal region.

3. Results

The meteorological conditions of summer 2002 determined the formation of five upwelling events, three in July (2/7, 10/7, 21/7) and two at the end of August (20/8, 27/8). The results presented here focus on the first days of each event in order to describe the prevailing meteorological (Section 3.1) and oceanic (Section 3.2) conditions in the beginning of the upwelling. The broader N. Aegean circulation and the BSW contribution on the evolution of the upwelling processes are presented in Section 3.3.

3.1. Meteorological conditions

Etesian winds prevailed during summer 2002, when 77% of the

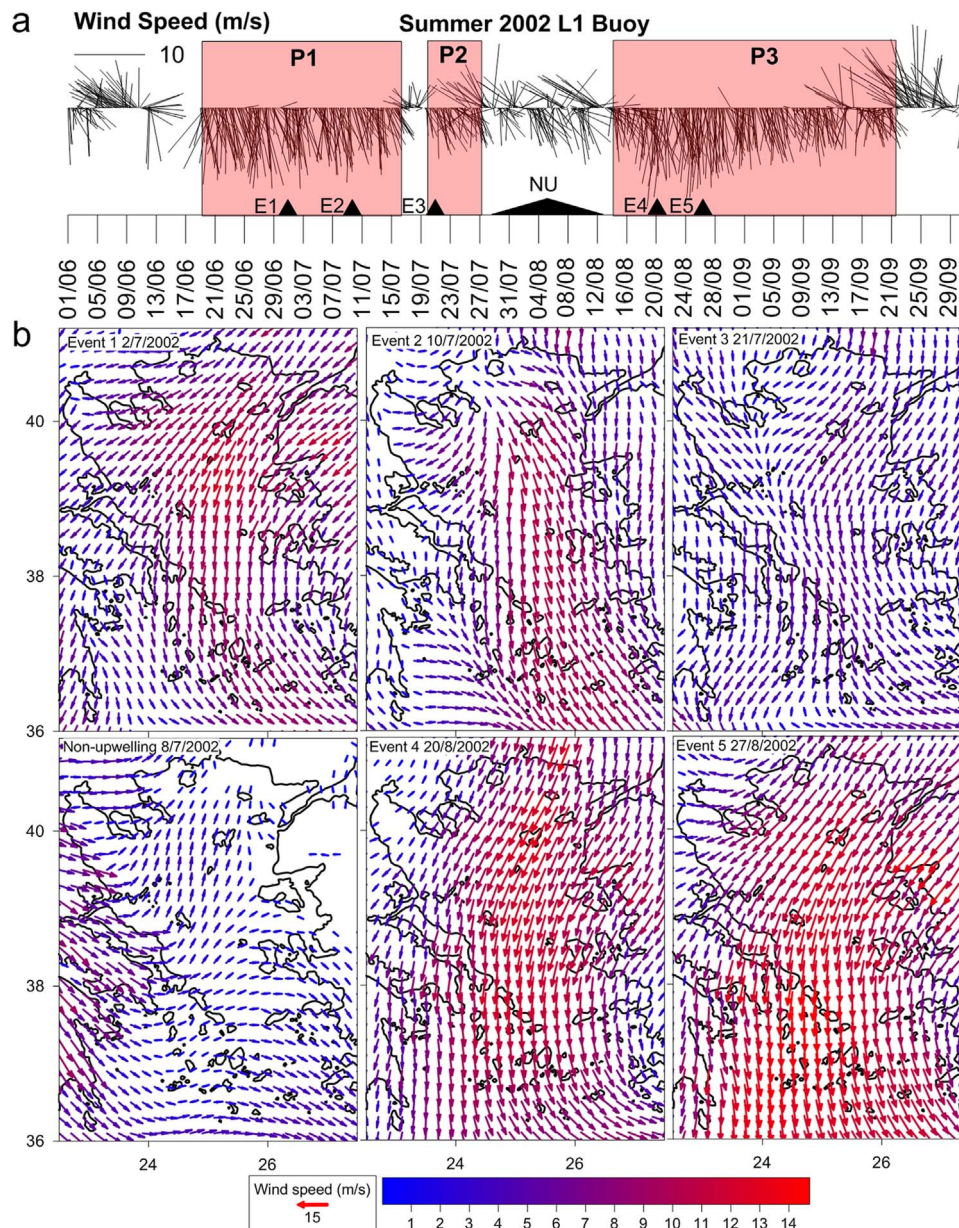


Fig. 3. Wind vectors (m/s) (a) temporal evolution, as measured from the Poseidon System at L1 buoy for summer 2002 and (b) snapshots of wind horizontal distribution, as derived from the Poseidon Forecasting System over the Aegean Sea on the first day of the five upwelling events (Events 1–5) and a period without upwelling (Non-Upwelling conditions: NU), indicated with black triangles. Three periods with continuous northerly winds are also marked (P1, P2 and P3). (For interpretation of the references to color in this figure legend, the reader is referred to the web version of this article).

summer winds measured at the L1 Poseidon Buoy originated from the North (northwesterly to northeasterly) (Fig. 3a). A first period (P1) of continuous northerly winds is detected from mid-June to mid-July, when winds greater than 10 m/s occurred, especially at the end of June and in the beginning of July. The horizontal distribution of simulated winds over the Aegean Sea, derived from the Poseidon Forecasting System in the first day of each upwelling event (see Section 3.2) is presented in Fig. 3b. The snapshots of wind distribution are related to the upwelling events and represent characteristic dates of strong upwelling favorable wind conditions. Very strong winds were simulated over the central Aegean and over the Lesvos area during P1 period (e.g. 2/7/2002 and 10/7/2002, Fig. 3b). Both wind snapshots of P1 period exhibit the known distribution of Etesian winds, with the characteristic turning of the direction over the central Aegean, from northeasterly to northwesterly direction. Although a short period of southerly winds appeared in mid-July (17/7/2002), a second period (P2) with upwelling favorable winds began a few days later (19/7/2002) and lasted

until 25 July (Fig. 3a). The respective horizontal distribution of the simulated wind fields (Fig. 3b) shows the domination of Etesian Winds over the entire Aegean Sea (21/7/2002). Strong variation between northerly and southerly winds occurred over the following period until mid-August, when several days with upwelling unfavorable conditions occurred (Fig. 3a). Easterly winds appeared over the western Aegean, turning to southeasterly over the Lesvos Island (e.g. 7/8/2002; Fig. 3b). However, a few days of northerly winds are appeared during the first 10 days of August (e.g. 1–5/8/2002 and 8/8/2002). A long third period (P3) with continuous strong northeasterly winds (> 15 m/s) over the Lesvos coastal area began a few days later, on 13 August (Fig. 3a); significant strong wind magnitudes occurred over the entire region, especially at the end of August (e.g. 20/8/2002 and 27/8/2002; Fig. 3b). A gradual reduction of the wind magnitude is observed in early September, while the northerly direction was completely vanished at the end of the month, when strong southerly winds prevailed over the Lesvos western coastal area (Fig. 3a).

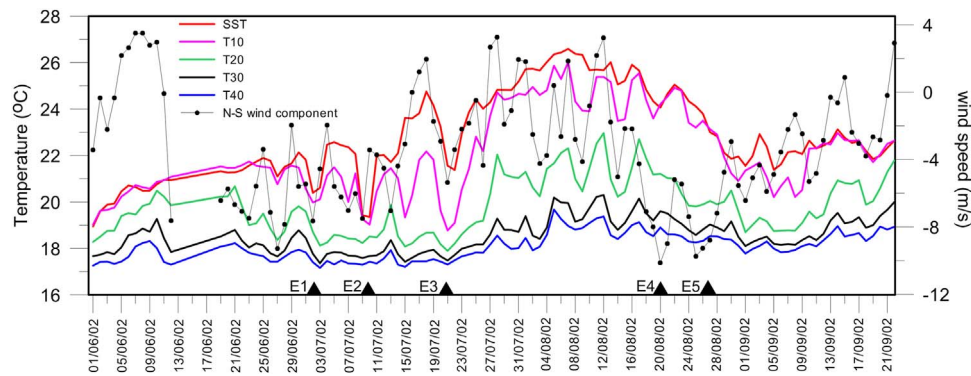


Fig. 4. Evolution of daily averaged temperature at the surface (SST), at 10 m, 20 m, 30 m and 40 m, as derived from Poseidon Buoy L1 (Fig. 1) measurements for summer 2002. The daily North-South (N-S) wind component (m/s), derived from L1 measurements is indicated with black dots; negative/positive values indicate the southward/northward direction of the wind component. The five upwelling events (E1, E2, E3, E4 and E5) are indicated with black triangles. (For interpretation of the references to color in this figure legend, the reader is referred to the web version of this article).

3.2. Upwelling events

The evolution of the sea temperature at several depths and the meridional component of the wind (N-S), as measured at L1 Poseidon Buoy during summer 2002, are presented in Fig. 4. Five significant SST drops are presented in both July and August, while a long period with very high surface values, without significant variation, is observed at the end of July and in early-August. More temperature drops were also measured at depths greater than 10 m (e.g. 2 August); however, SST remained high ($> 25\text{ }^{\circ}\text{C}$) without allowing the arrival of colder waters over the surface layers and therefore, we focus on the five temperature drops observed over the entire upper-ocean in both surface and subsurface layers. Specifically, two major upwelling events are detected on 2–4 July (Event 1) and 9–10 July (Event 2) during the first P1 period, when the surface temperature decreased by $2\text{ }^{\circ}\text{C}$ and $3\text{ }^{\circ}\text{C}$, respectively. In both cases, a respective simultaneous drop was also measured in 10 m depth. The temperature values in both surface and 10 m depth ranged over similar levels during both Event 1 ($\sim 20\text{ }^{\circ}\text{C}$) and Event 2 ($\sim 19\text{ }^{\circ}\text{C}$). The homogenization of the water column derived from the temperature vertical distribution (Fig. 4) is a strong indication of vertical mixing and upwelling that took place over the upper-ocean during these short periods, since water masses with similar temperature values are detected in both surface and sub-surface layers. Intense northerly winds prevailed in both cases, especially over the central Aegean, where wind speeds exceeded 15 m/s (Fig. 3b); the meridional component of the wind shows two negative peaks (-8 m/s ; Fig. 4) during these events, supporting the domination of strong northerly winds. A third upwelling event (Event 3) is detected a few days later from 19 July to 25 July, when both SST and temperature at 10 m decreased by $3\text{ }^{\circ}\text{C}$ (21 July; Fig. 4); SST reduced from $24\text{ }^{\circ}\text{C}$ to $21\text{ }^{\circ}\text{C}$, while the deeper 10 m layer showed a reduction from $22\text{ }^{\circ}\text{C}$ to $19\text{ }^{\circ}\text{C}$. The temperature drop signal is weaker but apparent in deeper layers, too; it is observed at 20 m depth ($\sim 1\text{ }^{\circ}\text{C}$) and weakens in deeper layers ($0.5\text{ }^{\circ}\text{C}$ at 30 m and $0.2\text{ }^{\circ}\text{C}$ at 40 m). The southward component of the wind dominates again, showing a strong negative value on 21 July ($\sim -5\text{ m/s}$). The first three events were formed during the P1 and P2 periods and appeared before the non-upwelling period of the high variable southerly winds (See Section 3.1). There is a notable correlation between the magnitude of the northerly winds and the SST levels at L1 location during summer of 2002. The Pearson correlation between measured wind magnitude and SST for summer days of 2002, when northerly winds occur, is $r = -0.6$ indicating the strong wind impact on the reduction of the surface temperature.

Temperature increased over all layers after 25 July and continued to increase until its highest values on 8 August following the summer atmospheric temperature increase (not shown). Meanwhile, strong southerly winds prevailed during this period over the western Lesvos

region (Fig. 3a). Northerly upwelling favorable winds are completely absent over the entire N. Aegean region during the temperature peak on 7 August (Fig. 3b). Despite the northerly upwelling favorable winds observed between 2 and 5 August (Figs. 3a and 4) and again on 8 August no upwelling occurred and surface temperature continued to increase. The broader oceanic conditions and especially the vertical structure during these days seemed to play an important role on this upwelling holdback (Section 4.2).

It is noted that the temperature levels at 20 m reached higher levels ($> 22\text{ }^{\circ}\text{C}$) than the highest SST values that occurred during the previous P1 period; the entire upper-ocean water column was warmed due to summer atmospheric conditions and upwelling absence. Sea temperature values remained at high levels until mid-August and showed a first significant reduction in both surface and greater depths around 20 August (Event 4). The reductions continued even more during the following days, when the strongest northerly winds of all summer occurred ($\sim 20\text{ m/s}$; Fig. 3a); the southward component of the wind revealed the highest magnitude of the entire period on 20 August ($> 10\text{ m/s}$). The temperature reduction slope and its values are almost identical in both surface and 10 m depth, reaching their lowest values between 27 August and 1 September ($\sim 22\text{ }^{\circ}\text{C}$, Event 5); strong favorable upwelling Etesian winds prevailed during this event over the entire domain (Fig. 3b) and the wind southward component is significantly strong ($\sim -10\text{ m/s}$). The northerly wind speed decreased by mid-September, but the following increase of the frequency of occurrence of southerly winds (Fig. 3a) mixed the upper layers, inducing same temperature values in surface and in 10 m at the end of September; no remarkable temperature drops occurred (Fig. 4), indicating the absence of upwelling.

3.3. BSW evolution under upwelling conditions

The SST distribution over N. Aegean region, as derived from the NAS-HYCOM simulations during the five upwelling events, is presented in Fig. 5. Maps of SST differences encountered between the NAS-HYCOM results and GHRSSST observations ($\text{SST}_{\text{NAS-HYCOM}}$ minus $\text{SST}_{\text{GHRSSST}}$) show small discrepancies between -0.5 and $0.5\text{ }^{\circ}\text{C}$ (white color in Fig. 5) in most of the N. Aegean areas. It is noted that the model overestimates the temperature of the BSW plume, especially at the proximity of the Dardanelles mouth. However, the BSW jet in front of the Dardanelles mouth is apparent on both NAS-HYCOM SST distribution and the satellite chl-a concentrations (Fig. 5), in agreement with Skliris et al. (2010), who showed that chlorophyll-rich and cold surface waters of Black Sea origin accumulate over the eastern N. Aegean region; BSW are characterized by higher chl-a content and therefore high chl-a distribution can be used to identify the evolution of the major BSW patterns, especially over northeastern Aegean Sea

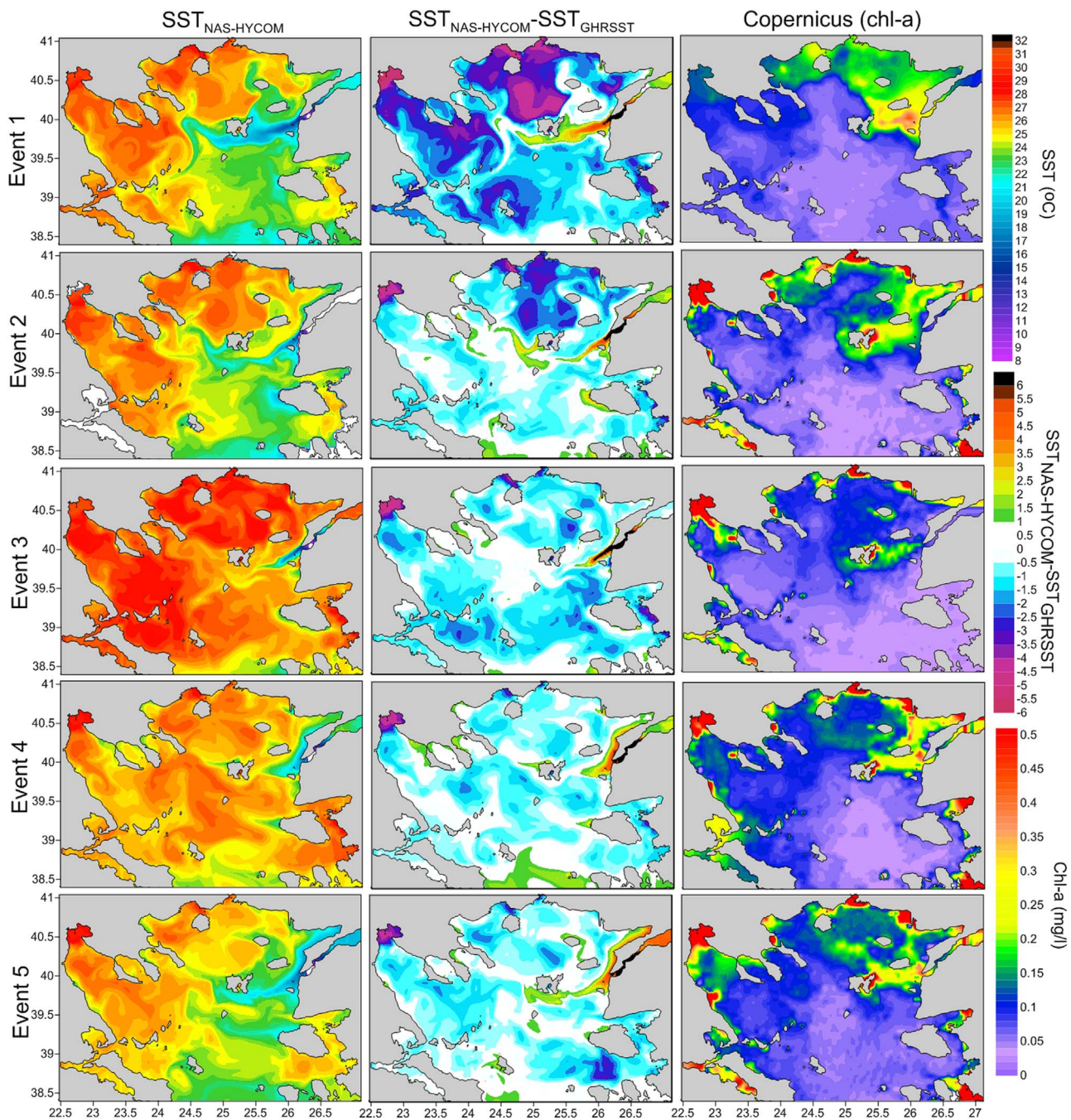


Fig. 5. Distribution of simulated SST (NAS-HYCOM), difference between NAS-HYCOM and GHRSSST SST ($SST_{NAS-HYCOM} - SST_{GHRSSST}$) and satellite chl-a (Copernicus) fields during the five study events over the N. Aegean domain. (For interpretation of the references to color in this figure legend, the reader is referred to the web version of this article).

(Tsiaras et al., 2012, 2014; Skliris et al., 2010). Large differences between GHRSSST and NAS-HYCOM fields also occur over some shelf and coastal regions (e.g. Thermaikos Gulf) in agreement with Xie et al. (2008), who showed that GHRSSST L4 products may show large uncertainties over coastal areas, especially shallower than 40 m. Although, large SST differences occur during Event 1, especially over the northern and northwestern region, the discrepancies are smaller over the southeastern area and the Lesvos upwelling region. Moreover, both satellite and model fields (small $SST_{NAS-HYCOM} - SST_{GHRSSST}$ differences), show colder waters over the surface along the eastern coasts, and especially over the western Lesvos region in most of the events in agreement with the high correlation between model and *in situ* time series presented in Section 2.3.2. (Fig. 2 and Table 1). The BSW propagated towards Limnos area at both Event 1 and 2 cases, but

remained near the Dardanelles mouth during Event 3. The low BSW discharge and the weak westward buoyant spreading are apparent in both NAS-HYCOM simulations and chl-a distribution. Low temperatures are observed over the western Lesvos coastal region, related to the upwelling Event 3, discussed in Section 3.2. Similarly, the westward spreading is also confined close to the Dardanelles mouth and over the northeastern Saros Gulf during Event 4; both NAS-HYCOM (SST) and satellite imaginary (chl-a) proclaim the intrusion of BSW inside this northeastern region; the high chl-a surface values observed over this enclosed gulf are related to the BSW intrusion since no strong river inputs occur inside the gulf in agreement with Androulidakis et al. (2012a, 2012b; based on simulations) and Pazi (2008; based on measurements), who showed that BSW may flow northward and enter into the Saros Gulf. On the contrary, Event 5 reveals strong south-

westward branch, south of Limnos, which is a common BSW circulation pattern under strong northerly winds and strong discharges (Androulidakis and Kourafalou, 2011). Cold waters, originated from the Lesvos upwelling region, also propagated towards the central region, as observed in simulated SST fields. Generally, almost all SST fields, presented in Fig. 5, support the known general temperature spatial distribution of the Aegean Sea during upwelling summer periods, with warmer (colder) temperatures over western (eastern) region (Zodiatis, 1994; Zervakis and Georgopoulos, 2002). However, the east-west increasing SST gradient characterizing the upwelling region in summer is not reflected in surface chl-a distributions (Fig. 5), in agreement with Skliris et al. (2010). Generally, in most upwelling regions, the upwelling waters are usually nutrient-rich and they are advected from below the thermocline, replacing the warmer, usually nutrient-depleted surface waters; the nutrient-rich up-welled waters then stimulate the growth and reproduction of primary producers, resulting in increased chl-a concentrations over the affected ocean surface. In the case of the Lesvos coastal region, we will show that the upwelling depth is relatively small and upwelling waters came from above the thermocline nutrient depleted layer (see Section 4.1), in agreement with Skliris et al. (2010). Therefore no major blooming events were triggered in the central and eastern Aegean during the five events of summer 2002; the chl-a satellite concentrations were low over the western Lesvos area during all study upwelling events (Fig. 5).

Significant salinity increases were measured at the L1 Poseidon Buoy during the 5 upwelling events, when the respective SST reductions occurred (Fig. 6). Contrastingly, the lowest salinity levels coincided with the SST peaks; the less saline waters occurred in the beginning of August 2002 (<36.5), when the warmest waters (~26 °C) of the entire study region covered the surface of the coastal region west of Lesvos. The simulated SST evolution follows the respective measured variation, especially during the upwelling events and during the non-upwelling period in late-July and early-August, when high surface levels occurred. The temperature levels are over-estimated, especially the high values during the non-upwelling period, but all reductions due to upwelling were captured by the model in agreement with the comparisons presented in Fig. 2. Similarly, the simulated salinity is underestimated in comparison with the measured values during June and September but it reveals smaller but respective reduction with the measured evolution at the end of July and in the beginning of August. There is a strong correlation between the measured SSS and SST time series during summer 2002, revealing high negative Pearson correlation coefficient ($r=-0.75$). Lower but also negative correlation is computed between the respective simulated SSS and SST time series ($r=-0.59$), indicating the good agreement between the simulated and measured findings.

The upwelling processes may supply the surface layers with colder and more saline waters, when waters with lower salinity are completely

absent. The salinity levels during Events 1 and 2 are already high since pre-existent waters were not affected by BSW intrusions, which would reduce the salinity of the surface masses. The signal of low salinity waters (<37) over the western Lesvos region is strongly related to waters of Black Sea origin, since normally N. Aegean waters reveal significant higher salinity levels (>39), especially over the southern N. Aegean region, due to the intrusion of S. Aegean waters (Poulos et al., 1997; Zervakis and Georgopoulos, 2002; Kourafalou and Barbopoulos, 2003). According to Nittis and Perivoliotis (2002), an average salinity value during the summer period in Lesvos is 38.8. Moreover, no other river brackish inputs exist close to the upwelling region; the closest river, Bakir River (Fig. 1), is located over the Turkish coasts and reveals very low discharge rates, especially during summer (<5 m³/s, Poulos et al., 1997). Therefore, the counter-correlation (negative coefficient) is related to periods of up-welled waters' appearance with lower temperature and higher salinity and of BSW intrusions, which in combination with the upwelling absence are characterized by lower salinity and higher temperature levels.

The simulated SSS distribution during the first (Event 1) and last (Event 5) upwelling event, and in two dates without upwelling processes (8/8/2002 and 16/8/2002) are presented in Fig. 7 in order to investigate the different BSW patterns between the two cases. The general cyclonic Aegean circulation led the surface waters away from the eastern N. Aegean region, keeping the brackish BSW over the northern and western N. Aegean region during the upwelling events; no brackish waters are observed over the central and southeastern region during Events 1 and 5 (Fig. 7a). In both events, although the Dardanelles outflow supplies the region with large quantities of waters, the buoyant BSW plume is restricted away from the upwelling region, supplying the general Aegean cyclonic circulation. Although northerly winds prevailed on 8 August, the strong southerly winds during the previous days (Figs. 3 and 4) formed an eastward branch of low salinity waters (Fig. 7b), originated from waters located along the Evia Island (Evia Jet; Androulidakis and Kourafalou, 2011). The southerly winds, over the N. Aegean Sea, may alternate the general cyclonic circulation along the Aegean coast and form an eastward spreading of low salinity surface waters, towards the central and southeastern region. These low salinity waters covered a part of the central region and may have formed a surface barrier layer over the broader upwelling region. Similarly, waters with lower salinity are presented over the southeastern region in mid-August (16/8/2002; Fig. 7b). Low SSS were measured on 16 August (SSS <37, Fig. 6), when although weak northerly winds dominated over the region (~5 m/s, Fig. 3a), upwelling processes are completely absent (SST >25 °C, Fig. 6). The combination of low salinity BSW, forming a surface barrier layer over the upwelling region, with weak northerly or southerly winds domination, consist a factor unfavorable for upwelling formation (see Section 4.1). On the contrary, the domination of strong northerly winds enhances the

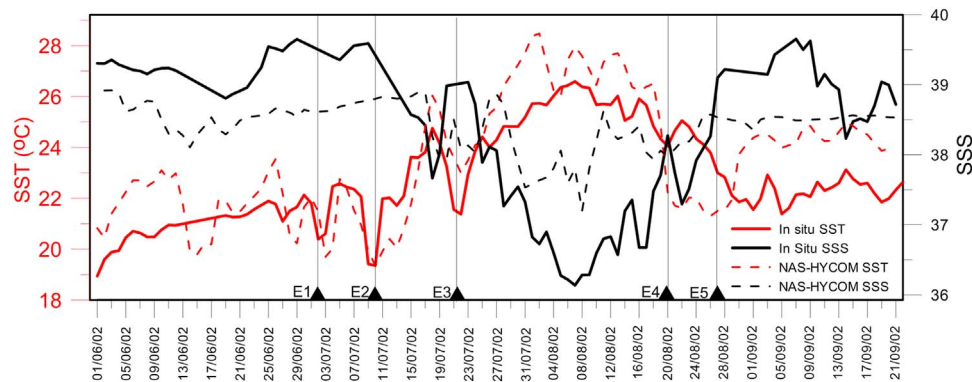


Fig. 6. Evolution of daily averaged Sea Surface Temperature (SST, red line) and Salinity (SSS, black line) as derived from Poseidon Buoy L1 (Fig. 1) measurements (solid line) and NAS-HYCOM simulations (dashed line) for summer 2002. The five upwelling events are indicated with black triangles and straight lines. (For interpretation of the references to color in this figure legend, the reader is referred to the web version of this article).

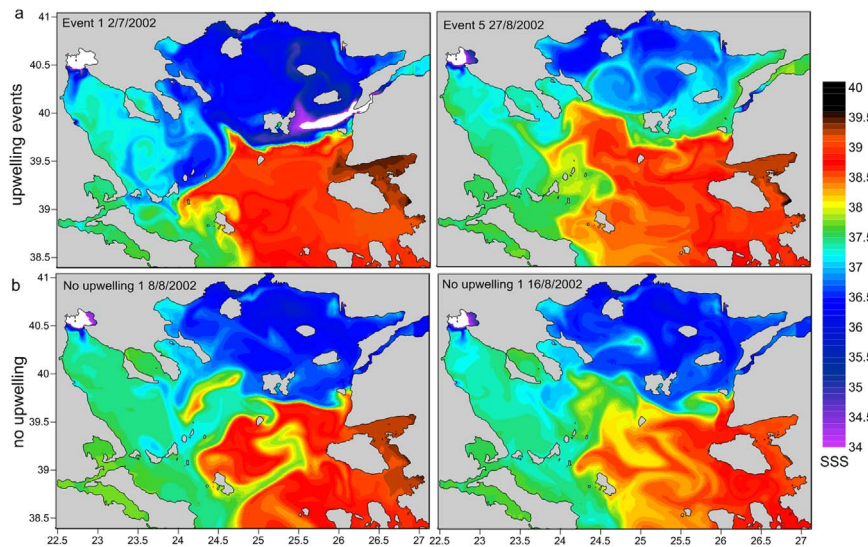


Fig. 7. Snapshots of Sea Surface Salinity (SSS) distribution as derived from the NAS-HYCOM simulations (a) during Events 1 and 5 and (b) on two characteristic days without upwelling (8/8/2002 and 16/8/2002). (For interpretation of the references to color in this figure legend, the reader is referred to the web version of this article).

cyclonic circulation along the coasts, keeping the brackish surface waters away from the upwelling region. Qu and Meyers (2005) showed that the barrier layer may prevent the transport of cold, nutrient-rich waters from below to the surface. With its steep gradient in density, the barrier layer enhances stratification so that upwelling and entrainment must be more intense to overcome the barrier layer's stability (Cabrera et al., 2011). However, a counter-argument to the barrier-role in a coastal region is that a thin overlying BSW layer could be displaced horizontally by Ekman transport towards the West (see Section 4.2).

4. Discussion

The vertical structure of the upper-ocean over the western Lesvos shelf region is strongly determined by the upwelling processes and the emersion of deeper, colder and denser masses towards the surface. The upwelling depth is an important factor of the physical and biochemical characteristics of the up-welled waters. The vertical distribution, the stratification, the Ekman transport and the upwelling depth during the study events of summer 2002 are discussed in the following section. The fate of the upwelling waters over the broader N. Aegean region and the interactions with the major Aegean circulation patterns are also under investigation with the use of simulated surface current fields and computation of Lagrangian drifters, based on the model output.

4.1. Vertical distribution and mixing

The simulated temperature and density vertical distribution of the upper 100 m, along a vertical section across the western Lesvos continental shelf (S1, Fig. 1), is presented in Figs. 8 and 9, respectively. In all study events, NAS-HYCOM simulations showed that colder waters from the upper intermediate layers (40–15 m) surfaced, while the pre-existing surface warmer waters are dragged offshore (Fig. 8). The density difference between the upwelling and the pre-existing waters varies between the upwelling events (Fig. 9). Event 1 presents a colder ($\sim 21^\circ\text{C}$; Fig. 8) and denser ($> 28\text{ kg/m}^3$; Fig. 9) mass that reached the surface from around 20 m depth. The surface layers were previously occupied by lighter ($\sim 27\text{ kg/m}^3$) and warmer (23.5°C) waters. Moreover, colder waters ($\sim 18.5^\circ\text{C}$), originating from 35 m, also reached the shallower layers ($\sim 15\text{ m}$) replacing the pre-existing warmer waters. The depth of the Ekman layer (D_E) is given by Eq. (3):

$$D_E = \pi \sqrt{\frac{2E_V}{|f|}} \quad (3)$$

Where E_V is the vertical eddy viscosity coefficient, derived from the NAS-HYCOM simulations at L1 location and f is the Coriolis parameter, equal with $f = 2\omega \sin \varphi$, where $\varphi = 39.22^\circ\text{N}$ (Latitude of L1 location). The depth of the Ekman layer removed due to the wind effect is around 15 m during Event 1 (Fig. 10a). This depth actually indicates the thickness of the surface water mass, replaced by colder deeper masses. Similarly during Event 2, cold waters ($\sim 19^\circ\text{C}$) from around 30 m depth (Fig. 8) occupied the upper 20 m (Fig. 10a). Upwelling processes are weaker during Event 3. Very warm surface waters ($> 26^\circ\text{C}$) were removed from the area during Event 3 and waters with relatively lower temperatures ($\sim 24^\circ\text{C}$) occupied the surface layers. The Ekman depth is quite small and equal to 10 m (Fig. 10a); however, slightly colder waters ($< 22^\circ\text{C}$) from 35 m moved upward, reducing the water temperature of the coastal area between 10 and 25 m (Fig. 8).

Strong stratification over the upper-ocean is observed under non-upwelling conditions on 8 August, when warm waters ($> 26^\circ\text{C}$) occupied the entire S1 Section, extended from Lesvos coast to central Aegean. The low density levels of the surface layers ($\sim 25.5\text{ kg/m}^3$; Fig. 9) is related to the warmer waters that covered the coastal region and also indicates the existence of an extended brackish barrier layer probably originated from the Black Sea in agreement with the very low salinity values measured in the surface of L1 buoy during the same period (Fig. 6),

Strong upwelling processes with larger Ekman depths (Fig. 10a) in comparison with the July events occurred at the end of August (Events 4 and 5; Fig. 8). Especially during Event 4, a thick and homogenous Ekman layer ($\sim 30\text{ m}$; Fig. 10a) was removed from the region, while colder waters occupied the coastal region. Deeper colder waters, originated between 20 and 30 m replaced the surface waters during these two successive events (Fig. 8). High temperature waters ($> 24^\circ\text{C}$) with density around 26 kg/m^3 , appeared only over the west edge of the section during Event 5.

The strong vertical mixing during upwelling events is indicated from the low values of the Brunt-Väisälä frequency (N stratification frequency) at L1 location, as derived from the NAS-HYCOM simulations and averaged over the upper 60 m (Fig. 10b). The stratification frequency reveals the vertical mixing ability of the waters between the model layers.

$$N^2 = \frac{(-g/\rho_0)(\rho_1 - \rho_2)}{\Delta z} \quad (4)$$

where g is the gravitational acceleration (9.806 m/s^2), ρ_0 is the initial

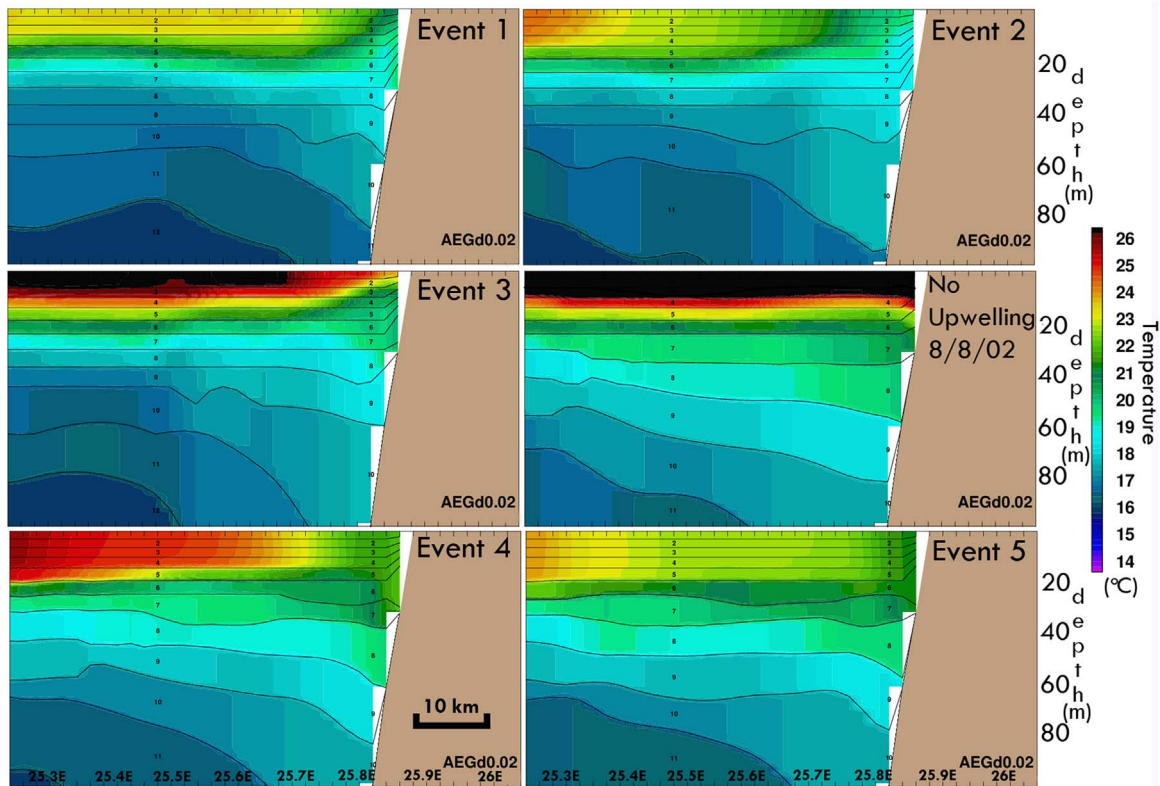


Fig. 8. Temperature vertical distributions along the S1 Section (Fig. 1) over the upper 100 m during the 5 upwelling events (Events 1–5) and during non-upwelling conditions (8/8/2002) of summer 2002. The contour lines indicate the hybrid layers of the NAS-HYCOM vertical structure. (For interpretation of the references to color in this figure legend, the reader is referred to the web version of this article).

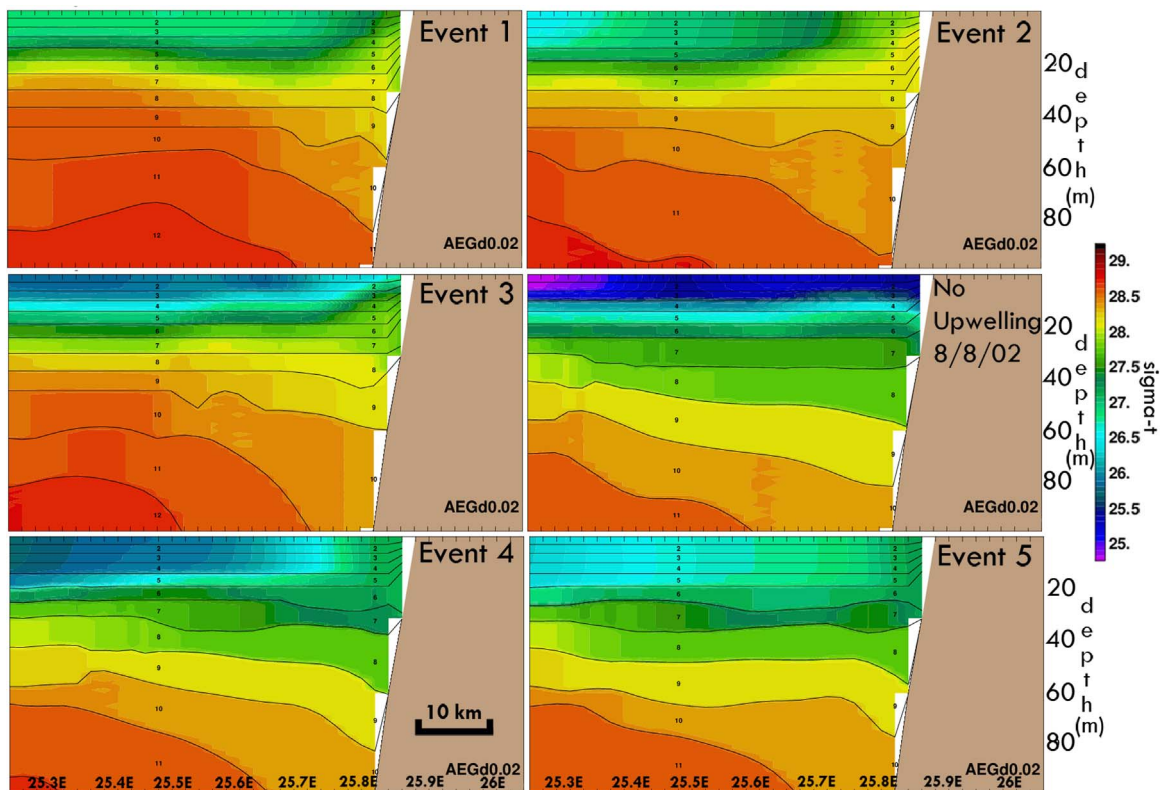


Fig. 9. Density ($\sigma\text{-t}$) vertical distributions along the S1 Section (Fig. 1) over the upper 100 m during the 5 upwelling events (Events 1–5) and during non-upwelling conditions (8/8/2002) of summer 2002. The contour lines indicate the hybrid layers of the NAS-HYCOM vertical structure. (For interpretation of the references to color in this figure legend, the reader is referred to the web version of this article).

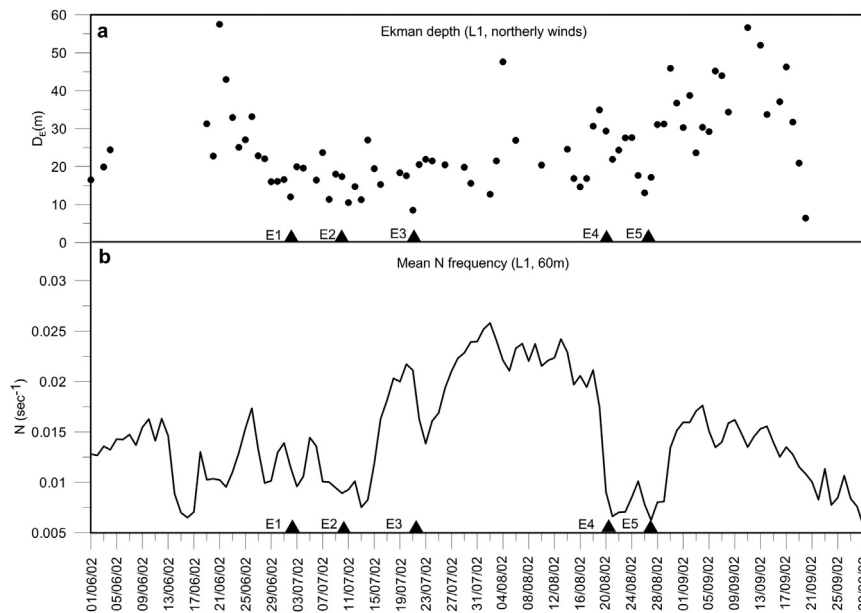


Fig. 10. Evolution of (a) Ekman layer depth (D_E ; dots) and (b) Brunt-Väisälä (N) stratification frequency (s^{-1}), averaged over the upper 60 m at L1 location (Fig. 1), as derived from NAS-HYCOM simulations in summer of 2002. The five upwelling events are indicated with black triangles.

ambient sigma-t, ρ_1 and ρ_2 are the upper and lower layer density, respectively, and Δz is determined by the thickness of the two successive model layers (distance between the layers' middles). The lowest stratification frequencies ($N \rightarrow 0$) are computed during the upwelling events, indicating the appearance of vertical homogenization over the upper 60 m. Three significant drops occurred in early-July, in agreement with the upwelling Events 1, 2 and 3, presented in the measured temperature time series (Fig. 4). The stratification formation, observed in mid-July, was sharply interrupted around 19 July, when the frequency decreased from $0.021 s^{-1}$ to $0.013 s^{-1}$, supporting the strong upwelling mixing and the vertical homogenization of the upper-ocean (Event 3). The stratification frequency distribution in late-July and in early-August shows strong stratification (large N) over the entire upper-ocean. However, it reduced significantly around 20 August, when northerly winds prevailed over the Lesvos region (Fig. 3). The lowest values ($< 0.075 s^{-1}$) appeared during Events 4 and 5, when strong upwelling occurred and the upper-ocean was covered with homogenous denser waters (Fig. 9). The low N values lasted until the end of August, when northerly winds began to weaken, upwelling was reduced and stratification was restored (high values in early and mid-September). The appearance of strong southerly winds in late September (Fig. 3a) mixed the upper-ocean and gradually reduced the N frequency (Fig. 10a). Another significant low appeared in mid-June ($N = 0.006 s^{-1}$) when especially the upper 10 m revealed very low N frequencies (Fig. 11a). Although upwelling was totally absent during this period (Fig. 4), SST and 10 m temperature levels were almost the same ($\sim 20.5^\circ C$). The prevailing southerly downwelling favorable winds probably mixed the surface layers and reduced the stratification frequency without inducing any upwelling.

The evolution of the vertical distribution of N frequency (Fig. 11a) shows high values ($N > 0.025 s^{-1}$) over the upper 20 m during non-upwelling periods (e.g. early-August). Weak stratification over the entire water column and especially over the upper 40 m is observed during all upwelling events in agreement with the average values presented in Fig. 10b. Although low values of mean N may result from the up-welled less stratified waters without necessarily active vertical mixing, the vertical distribution of stratification frequency and its low values at upwelling depths is a strong indicator of mixing and upwelling of deeper waters towards the surface layers. Significantly low values ($N \rightarrow 0$) are observed between 20–35 m, where the upwelling waters start to flow towards the surface during the first 3 events of July.

The stronger upward (positive) vertical velocities are observed between 20 and 40 m for all July events ($> 15 m/day$; Fig. 11b). Both Events 1 and 2 show upward velocities over the entire water column, while the weaker upwelling Event 3 showed lower or even absent upward velocities over the upper 25 m. Moreover, almost zero or negative (downward) vertical velocities are computed over the stratified upper 35 m during the non-upwelling period at the end of July and in the first half of August. Event 4 and especially Event 5 show low N frequencies over the upper 25 m inside the Ekman layer presented in Fig. 10a; the upward velocities were positive and strong over the upper 40 m indicating strong upwelling movement towards the surface layers.

In order to investigate if the low N levels result from the up-welled less stratified waters or from active vertical mixing of upwelling waters, the non-dimensional Richardson number (Eq. (6)) is also computed for each study case over the entire water column at L1 location.

$$Ri = N^2/S^2 \quad (6)$$

Where S is the squared horizontal velocity vertical shear:

$$S^2 = ((V_1 - V_2)/\Delta z)^2 + ((U_1 - U_2)/\Delta z)^2 \quad (7)$$

Where V_1, U_1 and V_2, U_2 are the horizontal components of the current velocity at two successive model layers with Δz vertical thickness, respectively. When the Richardson number is small ($Ri < 1/4$), the velocity shear is considered sufficient to overcome the tendency of a stratified fluid to remain stratified, and some mixing will generally occur. Otherwise if Ri is large, turbulent mixing across the stratification is generally suppressed (Turner, 1973). When the Richardson number is less than unity, it is an indication of artificial enhancement of vertical mixing. High Ri (> 10) occurred during non-upwelling conditions over the entire water column indicating that turbulent mixing across the stratification is generally suppressed. On the contrary, low Ri (< 1) occurred between 25 and 35 m during the 3 events of July in agreement with low N stratification frequency levels. The lowest Ri numbers are observed over the upper 20 m during Events 4 and 5, when enhancement of vertical mixing and upwelling took place.

The simulated temperature and density vertical distribution of two dates, one with extensive upwelling (Event 2) and one without upwelling in early-August (02/08/2002) are compared at L1 location. Both, temperature and density show very limited variation throughout the water column during Event 2, in comparison with the respective

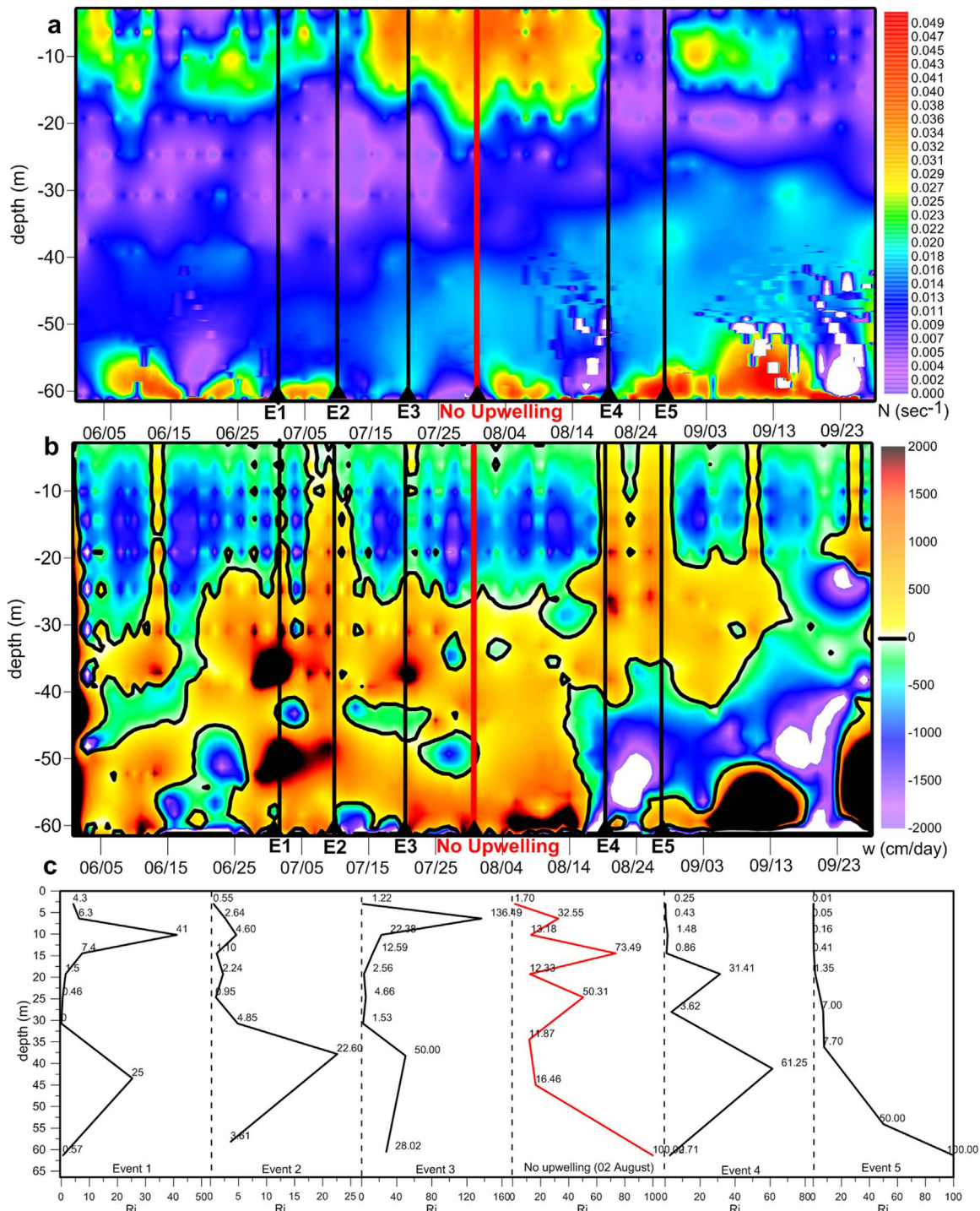


Fig. 11. (a) Hovmöller diagrams of summer stratification frequency N (s^{-1}), (b) vertical velocity (cm/day), and (c) vertical distribution of Richardson number (Ri) during the 5 upwelling events (Events 1–5; black lines) and during non-upwelling conditions (red line) over the upper 60 m at L1 location (Fig. 1), as derived by NAS-HYCOM simulation. (For interpretation of the references to color in this figure legend, the reader is referred to the web version of this article).

distributions on 2 August (Fig. 12a). A strong thermocline and a respective sharp pycnocline were simulated, when northerly winds were absent; temperature (density) significantly increases (decreases) over the upper 20 m from 20 °C (1030 kg/m^3) to 28 °C (1028 kg/m^3), in agreement with the summer stratification conditions of the N. Aegean region. Therefore, the stratification frequency shows almost stable vertical distribution, with very low values ($< 0.02 \text{ s}^{-1}$; Fig. 12b) along the entire water column under upwelling conditions (Event 2) and a distinct increase over the surface layers during the non-upwelling period (02/08/2002). It is noted that the lowest N values were

computed between 25 and 35 m in agreement with the upwelling depth of Event 2, derived from the Ri number vertical distribution presented in Fig. 11c; mixing is intense over this upper intermediate layer, where the denser waters moved towards the upper-ocean and finally reached the surface. On the contrary, on 2 August, the stratification frequency is larger ($> 0.01 \text{ s}^{-1}$) than the respective upwelling distribution, especially over the upper 50 m. Stratification frequency increases towards the surface due to the seasonal thermocline formation and the appearance of low salinity BSW ($\sim 0.04 \text{ s}^{-1}$).

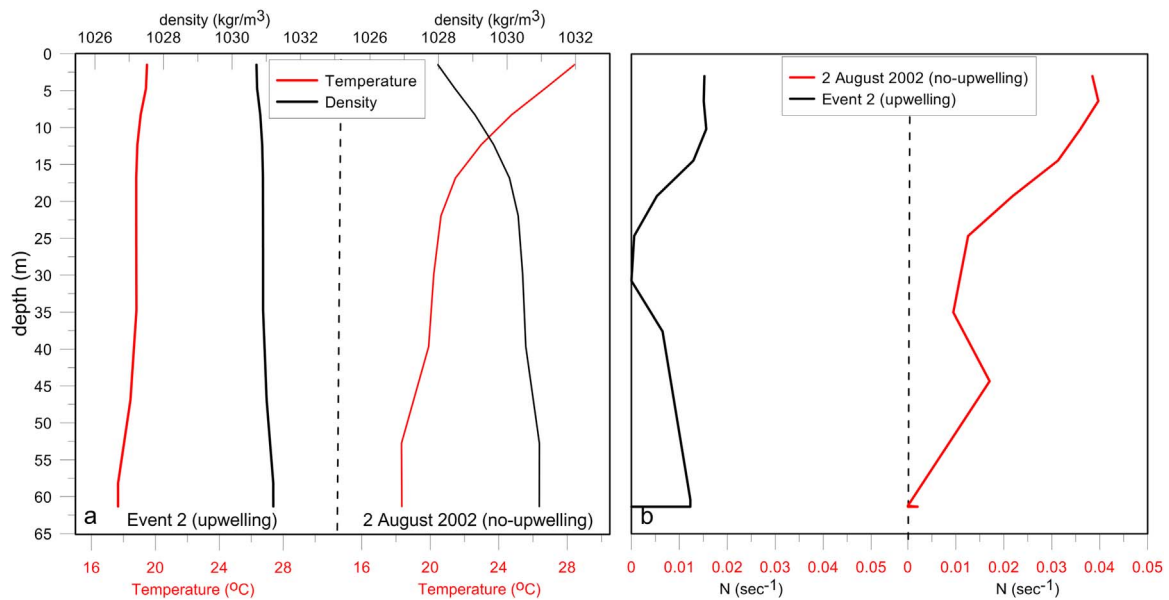


Fig. 12. Vertical distribution of (a) density (kg/m^3 ; black line), temperature ($^{\circ}\text{C}$; red line) and (b) N stratification frequency (s^{-1}) at L1 location (Fig. 1), as derived from NAS-HYCOM simulations under upwelling (Events 2) and non-upwelling (02/08/2002) conditions. (For interpretation of the references to color in this figure legend, the reader is referred to the web version of this article).

4.2. Circulation features during upwelling events

The westward water transport, induced by the upwelling Ekman transport is strongly related to the integrated current velocity over the Ekman layer. Therefore, we computed the velocity of the integrated Ekman current (V_E) at L1 position in summer 2002. The Ekman velocity is a function of wind stress:

$$V_o = \frac{\pi\sqrt{2}\tau_s}{D_E\rho|f|} \quad (5)$$

where ρ is the vertical integrated density of the Ekman layer, derived by the NAS-HYCOM simulations. Wind stress τ_s was derived from the atmospheric forcing used in the NAS-HYCOM simulations (Section 2.3.1). The red line in Fig. 13a illustrates the daily evolution of the magnitude of the Ekman current under upwelling favorable northerly winds. The magnitude of the Ekman current shows high peaks during all 5 upwelling events (red line in Fig. 13a). Significantly strong current

is observed during Event 1, when the prevailing direction was south-westward and its magnitude ranged around 10 cm/s. Similarly, strong Ekman current is also observed during Event 5 (~8 cm/s), where the Ekman layer is thin (< 20 m; Fig. 10a) and it is more easily displaced by the wind. Northward Ekman current was appeared at the end of July, when the wind revealed strong northward component (Fig. 4) and upwelling was totally absent. Although northerly winds prevailed during the first days of August (e.g. 1–5/8/2002), the Ekman current is very weak (< 4 cm/s) without generating upwelling formation as presented in the temperature evolution illustrated in Fig. 4.

The integrated transport over the Ekman depth across the S4 section (east-west transport, Q_{S4}) shows the eastward (westward) propagation of waters towards (away from) the upwelling region (Fig. 13b). Westward (negative) flow is observed during all upwelling events, while eastward flow prevailed during non-upwelling periods (late July-early August). This eastward flow brought low salinity waters of Black Sea origin towards the Lesvos region and even blocked the

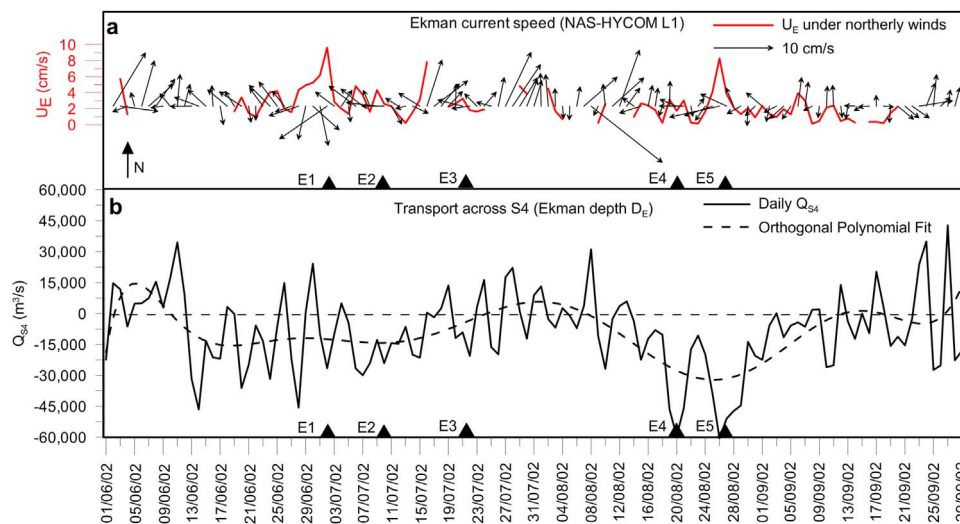


Fig. 13. Evolution of (a) Ekman layer current speed (U_E ; red line) under northerly winds and daily current vectors (black arrows) at L1 location (Fig. 1), and (b) Q_{S4} transport (m^3/s) across S4 section (Fig. 1b), as derived from NAS-HYCOM simulations in summer 2002. Positive (negative) values indicate eastward (westward) transport averaged over the Ekman depth. The orthogonal polynomial fit (10th order) of Q_{S4} transport is also presented (dashed line). (For interpretation of the references to color in this figure legend, the reader is referred to the web version of this article).

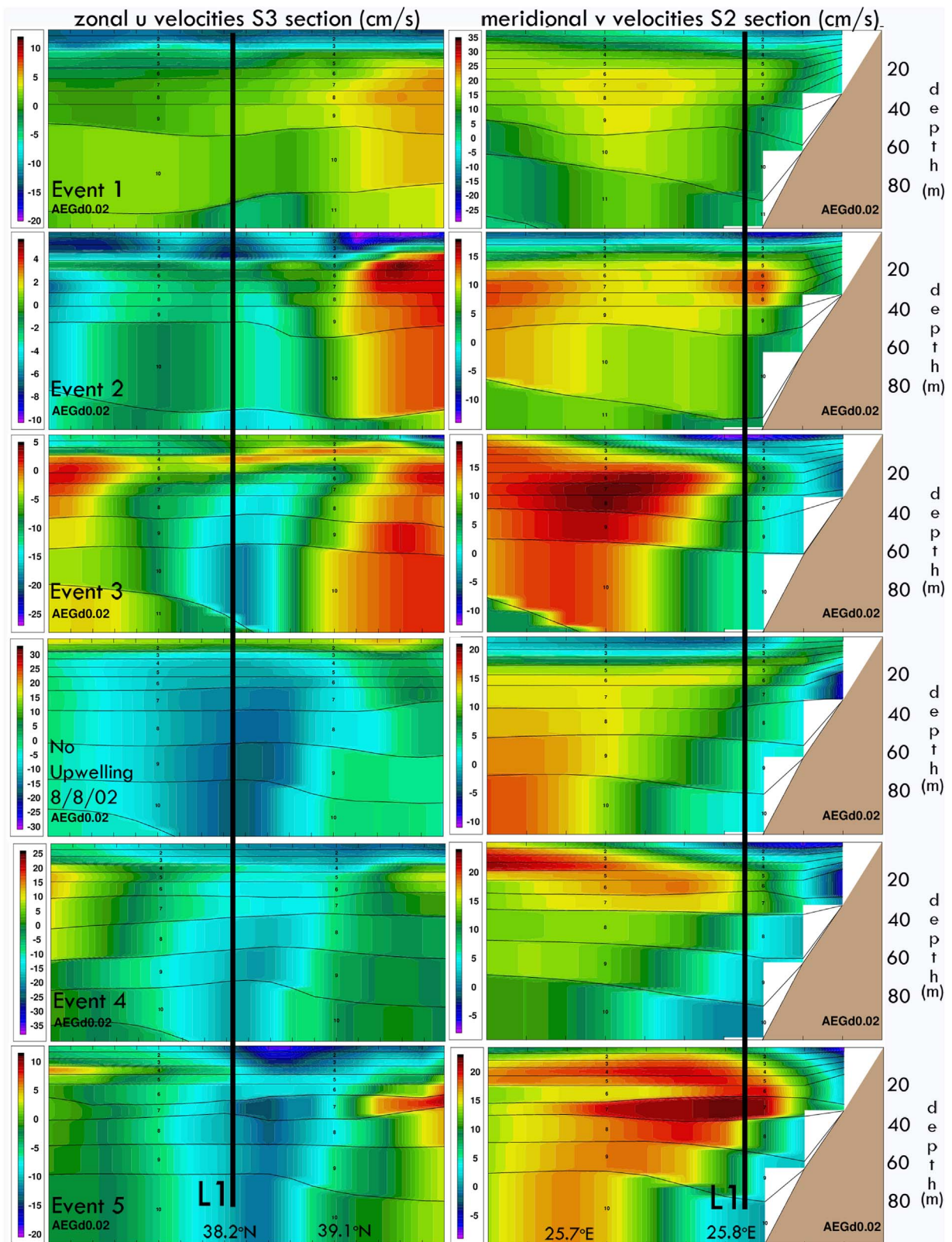


Fig. 14. Vertical distribution of zonal and meridional velocities (cm/s) along the S3 and S2 Sections (Fig. 1b), respectively, over the upper 100 m during the 5 upwelling events (Events 1–5) and during non-upwelling conditions (08/08/2002) of summer 2002, as derived from NAS-HYCOM simulations. The location of L1 buoy is indicated with a black solid line. The contour lines indicate the hybrid layers of the NAS-HYCOM vertical structure. (For interpretation of the references to color in this figure legend, the reader is referred to the web version of this article).

Ekman westward transport when upwelling favorable conditions occurred (e.g. 1–5 August). The highest positive (eastward) value occurred on 8 August 2002 (~30,000 m³/s; Fig. 13b), when a jet of low salinity waters formed towards the East and reached the upwelling region as presented in Fig. 7b.

The vertical distribution of zonal velocities across Section S3 (Fig. 1b) shows the eastward transport (positive values in Fig. 14) over the surface layers on 8 August 2002. A clear eastward surface jet with very high velocities (> 20 cm/s) is observed in the southern part of the section. On the contrary, westward transport is observed over the surface layers during Events 4 and 5, when strong upwelling took place. The strong westward velocities (negative values in Fig. 13) represent the westward component of the Ekman current during all upwelling events. The westward current was also strong and extensive, covering the entire S3 Section with velocities around 15 cm/s during Event 1. The southward alongshore component of the Ekman transport is also apparent in the distribution of the meridional velocities along the S2 Section (Fig. 14). Negative values (southward velocities) cover the upper layers, close to the Lesvos coast during all upwelling events. This is not the case on 8 August 2002, when positive (northward) velocities occurred very close to the coast. The 10th order polynomial fit of the Q_{S4} transport (dashed line in Fig. 13b) describes the variability of the eastward-westward flow with negative values in early and mid-July, positive values at the end of July and early-August, and a strong negative drop at the end of August. The blocking effect on the westward

Ekman transport due to the intrusion of broader open sea waters towards the coastal region in combination with the formation of low salinity barrier layer suppressed any upwelling processes that would occur under upwelling favorable conditions.

In order to investigate the fate of the up-welled waters under the effect of different N. Aegean circulation features, synthetic drifter tracks of modeled surface floats (Lagrangian floats) were launched at L1 location over the western coastal zone of Lesvos (Fig. 15). The computation of drifter tracks, based on the NAS-HYCOM velocity fields, followed the methodology by Garraffo et al. (2001). Several differences between the simulated drifter tracks of each upwelling event are observed due to the general circulations features that dominated over the N. Aegean. In all upwelling events, the incipient movement of the drifters is westward, following the general south-westward circulation over the eastern region, under strong northerly winds. The distribution of the simulated surface circulation, averaged over the first 10-days (10-d) period after each upwelling event, is also presented in tandem with the entire drifter track. The distinct BSW propagation features are presented in all cases, forming usually a branch, southward of Limnos islands (SW Branch), due to northerly winds forcing and strong Dardanelles outflow rates in agreement with Androulidakis and Kourafalou (2011). Several N. Aegean known circulation patterns, such as the general cyclonic circulation along the coasts (Yüce, 1995) with the Rim Current south of Chalkidiki Peninsula and the southward current along the Evia Island (Evia Jet) are

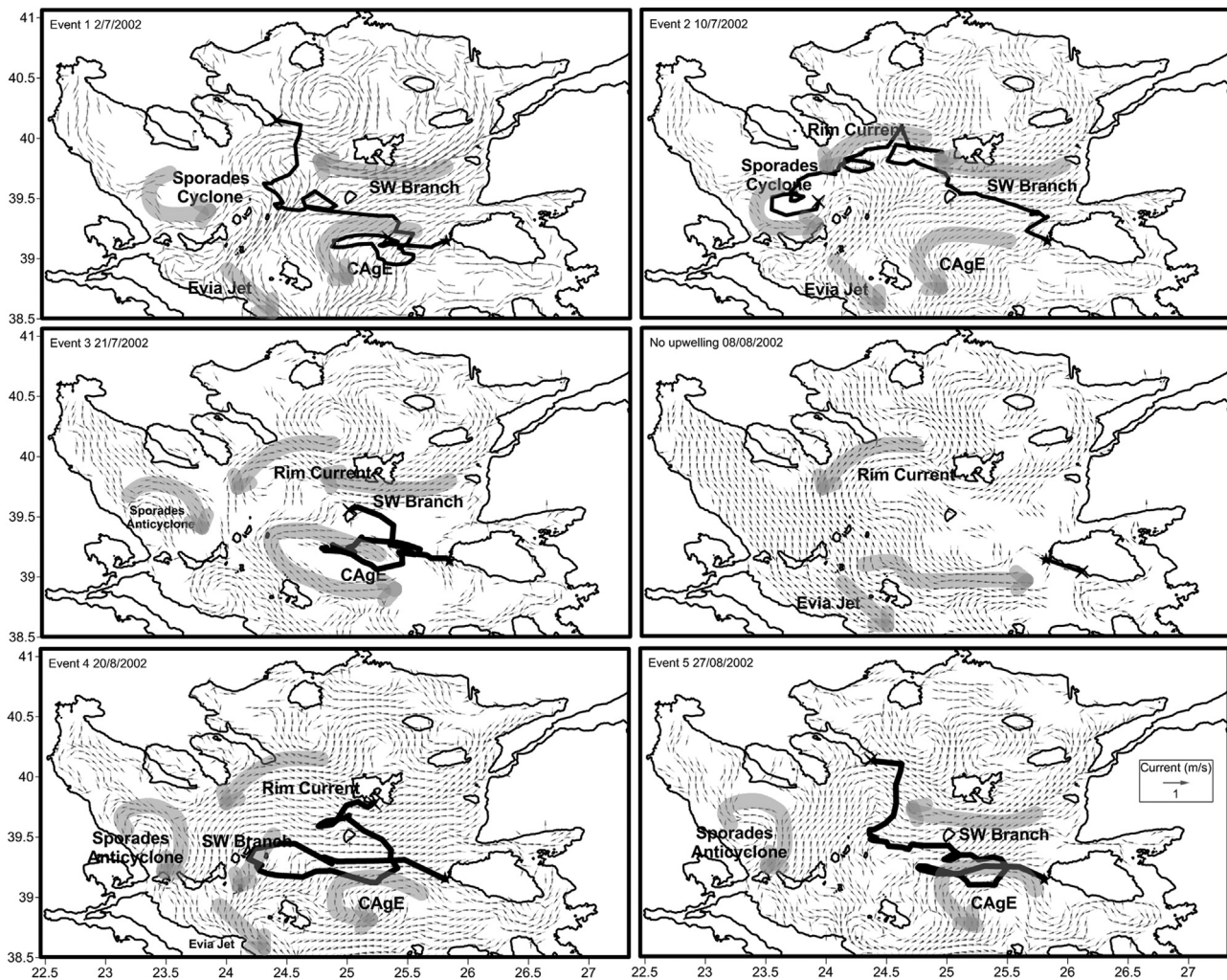


Fig. 15. Distribution of mean 10-day surface currents and simulated surface drifters for a 10-day period, deployed at the location of L1 station (black star), on the first day of the five upwelling events (Events 1–5) and on a day without upwelling (08/08/2002). Several N. Aegean circulation features (Evia Jet, SW Branch, Sporades Anticyclone and Cyclone, Rim Current and Central Aegean Cyclone-CAGe) are indicated. Currents below 5 cm/s are excluded (white areas).

adequately simulated by NAS-HYCOM. The Sporades anticyclonic eddy (Sporades Anticyclone; Olson et al., 2007), which usually forms in autumn, is also apparent at the end of summer (Events 4 and 5). The cyclonic circulation over the central and southeastern region is part of the permanent cyclonic Chios Gyre (Nittis and Perivoliotis, 2002; Olson et al., 2007). Sayın et al. (2011), showed that this cyclonic circulation, west of Lesvos Island, appears usually during summer, forming a distinct CAgE (Central Aegean Eddy), north of the Chios Gyre. NAS-HYCOM simulations adequately simulated the CAgE in the proximity of the Lesvos upwelling area during all upwelling events (Fig. 15).

The simulated drifter launched in the first day of Event 1 was dragged by the southwestward currents and intruded inside the CAgE, following the cyclonic turn of the eddy; its implication with the SW Branch of the BSW plume led it towards the West and finally over the Athos Basin. This result supports the transport of waters from the Lesvos coastal upwelling area to the north-central Aegean, where low salinity BSW usually prevail over the surface layers (Fig. 7b). Although the mean 10-d surface circulation over the Sporades and Athos basins was characterized by the southwestward Rim Current, the drifter propagation over this specific area is northward due to possible short changes in the general surface circulation that cannot be captured and shown in the 10-d means. However, during its last days, it turned to the West due to the prevailing westward circulation south of the Athos Peninsula.

The drifter fate is similar during Event 2, without the entrainment inside the CAgE, since the initial movement of the drifter was more to the North, where BSW westward current prevailed (SW Branch), dragging surface waters south of Limnos and along the Rim Current, towards the Sporades Basin. The drifter was entrained inside a cyclonic eddy over the Sporades Basin (Sporades Cyclone), which is a competitive feature to the Sporades Anticyclone (Kourafalou and Barbopoulos, 2003). The weakest northerly winds between all study upwelling events were observed during the P2 period (Fig. 3a), when Event 3 occurred; the distribution of the surface circulation during the first 10 days shows a weaker westward spreading of surface waters, over the central region in comparison with the other events. Therefore, the drifter moved to the West and implicated only with the CAgE, remaining over the central region.

The absence of continuous northerly winds during the non-upwelling period (Fig. 3) induced totally different circulation patterns, especially over the south central region. Although the major Aegean cyclonic circulation is apparent (e.g. Rim Current, Evia Jet) the westward surface spreading is absent. Low salinity waters (Fig. 7b), carried by an eastward current, derived from the general cyclonic circulation (Fig. 15) and covered the broader southern region. The simulated float was dragged eastward towards the southern Lesvos coast, supporting the movement of surface waters towards the Southeast.

The westward propagation of the surface drifters is again apparent during Events 4 and 5 under the effect of the cyclonic CAgE circulation pattern. The Event 4 drifter moved towards the Sporades Islands, where the surface waters propagated towards the South, interrupting the westward movement of the drifter. This finding agrees with Androulidakis and Kourafalou (2011), who showed that BSW may cross the Skyros Basin and supply directly the Evia Jet (as opposed to traveling around the entire N. Aegean), under strong northerly winds during summer; northerly winds are significantly strong during Event 4 (Fig. 3). The Event 5 drifter followed the spreading of the up-welled waters over the central region, as presented in the SST distribution (Fig. 5). Finally, it moved towards Limnos Island and finally over the Athos Basin, after its involvement with the CAgE, which seems to be a permanent feature over the south-central region. A short northeastward switch of its track over the western Limnos area is probably related to its implication with the SW Branch, which carried surface waters south of Limnos and towards the Athos Basin, determining the fate of the drifter. The initial movement of the drifter due to the

domination of the cyclonic eddy over the Central region (CAgE) describes the prevailing circulation pattern of the up-welled waters over the broader N. Aegean.

4.3. Dissolved oxygen variability

It is shown that the upwelling processes for all events took place within the upper 40 m, indicating that the up-welled masses over the western Lesvos region include waters from the subsurface layers of the Aegean Sea. Herein, we use Dissolved Oxygen (DO) measurements to confirm the origin of the up-welled waters and investigate their differences with pre-existing surface masses. Lykousis et al. (2002), based on research cruises, showed that the subsurface layer (20–50 m) of the N. Aegean Sea may show higher DO concentrations than the surface and deeper layers (their Fig. 6a). Although BSW exhibits relatively high oxygen concentrations, especially during spring, Souvermezoglou et al. (2014) have showed that the surface layers of the broader Lesvos and Limnos regions may reveal lower average levels than the deeper intermediate layers during August–September–October (table 3 by Souvermezoglou et al. (2014)). In this work, DO concentration measurements ($[O_2]_{meas}$) from the surface of L1 Poseidon Buoy were used. The Apparent Oxygen Utilization (AOU) is defined as the difference between the equilibrium, or solubility, value of oxygen ($[O_2]_{eq}$) and the measured concentration.

$$AOU = [O_2]_{eq} - [O_2]_{meas}$$

where $[O_2]_{eq}$ is the solubility value for the measured temperature and salinity of the water sample in the surface of L1 buoy, according to Garcia and Gordon (1992), and $[O_2]_{meas}$ is the respective measured oxygen concentration of the surface sample. By definition AOU removes the effect of oxygen solubility, which is primarily driven by temperature (Garcia et al., 2005). Negative values indicate regions in which the dissolved oxygen concentration is elevated above its equilibrium saturation concentration typically observed in near-surface euphotic waters. The negative AOU values of surface waters indicate that productivity-related changes in oxygen concentration are more pronounced in these surface layers, which makes the measured oxygen higher than that of theoretical values (Gopinath et al., 2006).

The evolution of the AOU anomaly (the difference between the AOU, derived from the 3-hourly measurements, and the AOU summer mean) during summer 2002 is presented in Fig. 16. We calculated the AOU anomaly to avoid possible bias of the available measurements due to sensor and instrument maintenance failures and to focus on the variability of the oxygen surface levels in relation to the upwelling events of summer 2002. The majority of the summer values ranged between 0 and $-20 \mu\text{mol/kg}$, revealing a general increasing trend from June to August. A strong increase occurred in September, when positive AOU anomaly was computed. However, significant negative peaks of AOU anomaly ($\sim -30 \mu\text{mol/kg}$) are observed during all upwelling study events (indicated with dashed circles in Fig. 16a). On the contrary, AOU anomaly increases, when upwelling processes are suppressed and the surface layer is covered by low salinity (Fig. 6) waters of Black Sea origin. The AOU anomaly increase, observed in mid-July ($\sim 15 \mu\text{mol/kg}$), was interrupted by Event 3, when upwelling waters reached the surface. The low AOU anomaly value on 21 July ($-25 \mu\text{mol/kg}$) coincides with the low temperature of 21°C , while the entire SST variation is a mirror image of the AOU anomaly evolution, during a 6-days period of Event 3 (Fig. 16b). Higher SST values ($> 24^\circ\text{C}$) were measured after the upwelling (24 July), when AOU anomaly ranged at positive values, influenced by the broader surface waters. The Pearson correlation coefficient of 3-hourly AOU and SST measurements in the surface of L1 Buoy, from 19 July until 25 July (Event 3) is high and positive ($r=0.75$), indicating the strong relation between the up-welled waters and the variation of the dissolved oxygen surface concentrations (Fig. 16). The correlation between the surface AOU anomaly negative values and SST values is strong during all

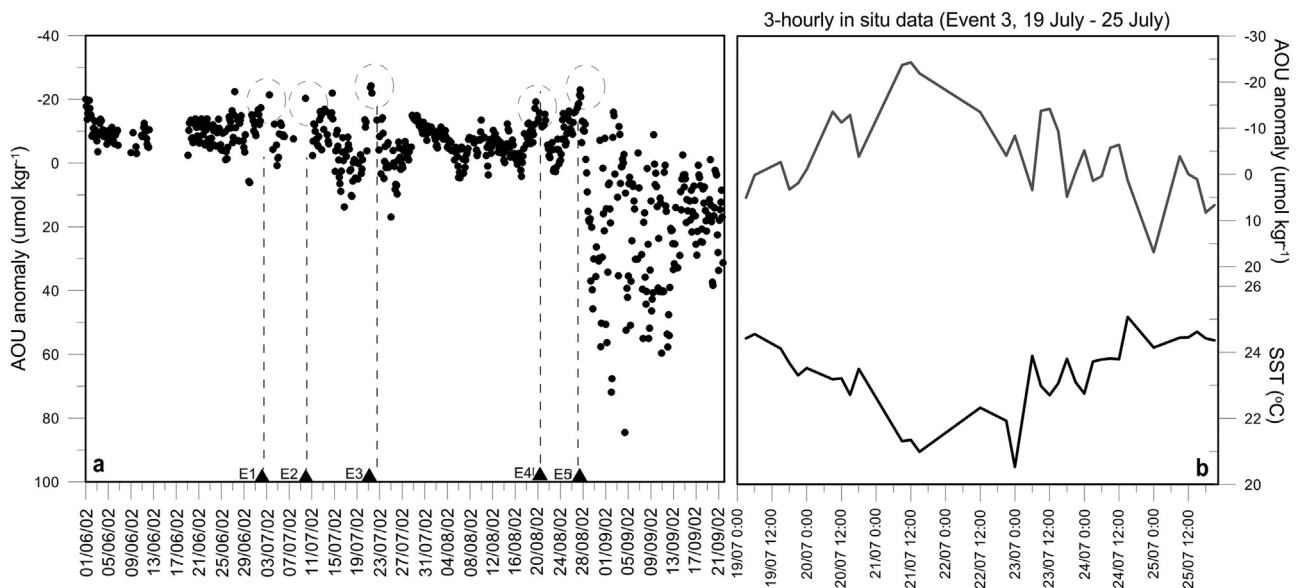


Fig. 16. Evolution of (a) daily Apparent Oxygen Utilization (AOU) anomaly for summer 2002 and (b) 3-hourly AOU anomaly and SST evolution during Event 3, as derived from measurements of L1 Poseidon Buoy (Fig. 1). The five upwelling events are indicated with black triangles and dashed lines.

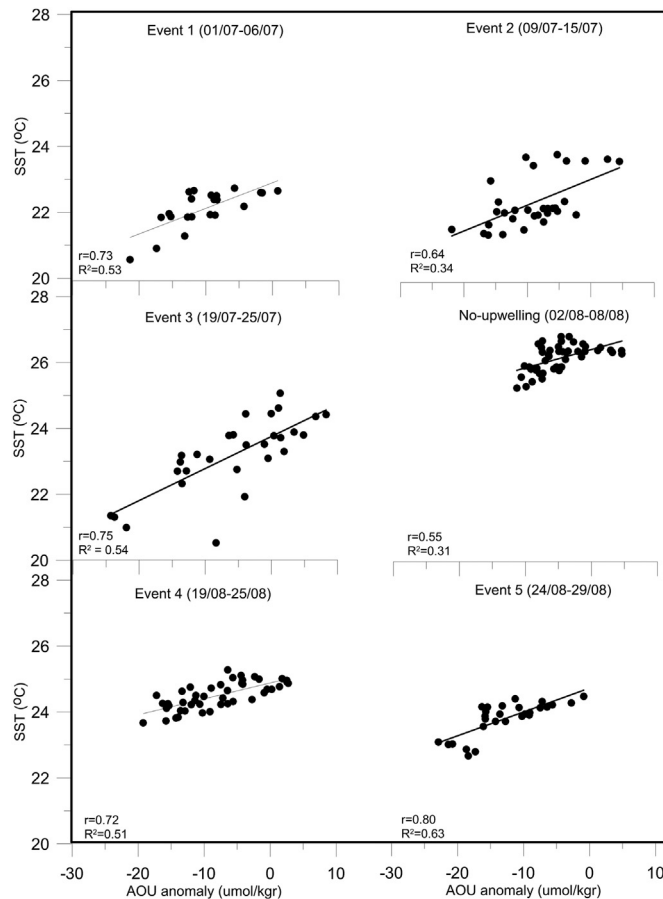


Fig. 17. Scatter diagrams of Sea Surface Temperature (SST) and Apparent Oxygen Utilization (AOU) anomaly, as derived from 3-hourly measurements at L1 Poseidon Buoy during the 5 upwelling events (Events 1–5) and during non-upwelling conditions (02/08-08/08) of summer 2002. The linear fit (solid line), the Pearson Correlation Coefficient (r) and the R^2 are also presented for each case.

upwelling events (Fig. 17), showing positive and very high Pearson coefficients ($r > 0.60$), and relatively high R^2 values (Steel and James, 1960) indicating the good fit between the two time series. However, relatively lower correlation coefficient ($r=0.55$) and R^2 (0.31) were

computed for the non-upwelling period (02/08-08/08). Higher AOU anomaly ($> -10 \mu\text{mol/kg}$) are observed in the first half of August (Fig. 17), when upper-ocean stratification is strong (Fig. 10b). Two significant negative peaks are also observed during Events 4 and 5 (Fig. 16a), when upwelling waters reached the surface of the Lesvos region. It is noted that the up-welled waters, originated from the subsurface layers, reveal lower AOU values (negative peaks) and thus are characterized of dissolved oxygen concentrations that are more elevated above their equilibrium saturation concentration in comparison with the pre-existent surface waters.

Recent CTD measurements in Autumn 2013 (see Section 2.1), in the proximity of the Dardanelles mouth (AMT5), over the central N. Aegean region (AMT8) and between Samothraki and Limnos Islands, showed very low surface DO concentrations ($< 5.3 \text{ ml/l}$; Fig. 18a). The upper 30 m were covered by low salinity waters affected by the BSW discharge (Fig. 18b); surface salinity was very low especially in front of the Dardanelles mouth (AMT5) and increased with depth, indicating the thickness of the BSW plume ($\sim 40 \text{ m}$). The temperature vertical distribution revealed warmer waters over the upper 40 m due to the previous summer conditions, while a small surface layer ($< 10 \text{ m}$) in front of the Dardanelles mouth (AMT5) showed lower temperature levels due to the autumn atmospheric conditions, which reduced the surface layer temperature especially in Black Sea and along the Turkish Straits. Although the surface temperature was still higher ($\sim 21 \text{ }^\circ\text{C}$) over the northern (AMT1) and southern (AMT8) stations, the BSW plume was also apparent with salinity levels around 35 and 38 units, respectively. The temperature levels decrease with depth, especially below 20 m (AMT8) and 40 m (AMT1). At AMT8 station, close to the Lesvos Island, the DO surface levels range below 4.4 ml/l , but increase with depth, revealing a high peak at 35 m ($\sim 5.3 \text{ ml/l}$) below the BSW plume. Similarly, the northern AMT1 profile, located along the north-westward BSW branch (Androulidakis and Kourafalou, 2011) showed DO concentrations peak ($\sim 5.6 \text{ ml/l}$) and low temperature levels ($< 18 \text{ }^\circ\text{C}$) at 50 m depth. In all cases, the DO started to increase at around 15–40 m, while DO concentration levels decreased again below 70 m depth. Although the 3 stations showed different DO variability, all profiles revealed a similar variation with depth, indicating the BSW DO differences in comparison with the subsurface layer between 15–50 m. These results agree with the upwelling depth over the Lesvos region, where colder waters with larger DO concentrations $[O_2]_{meas}$ and lower AOU values, originated from layers below 15 m and shallower

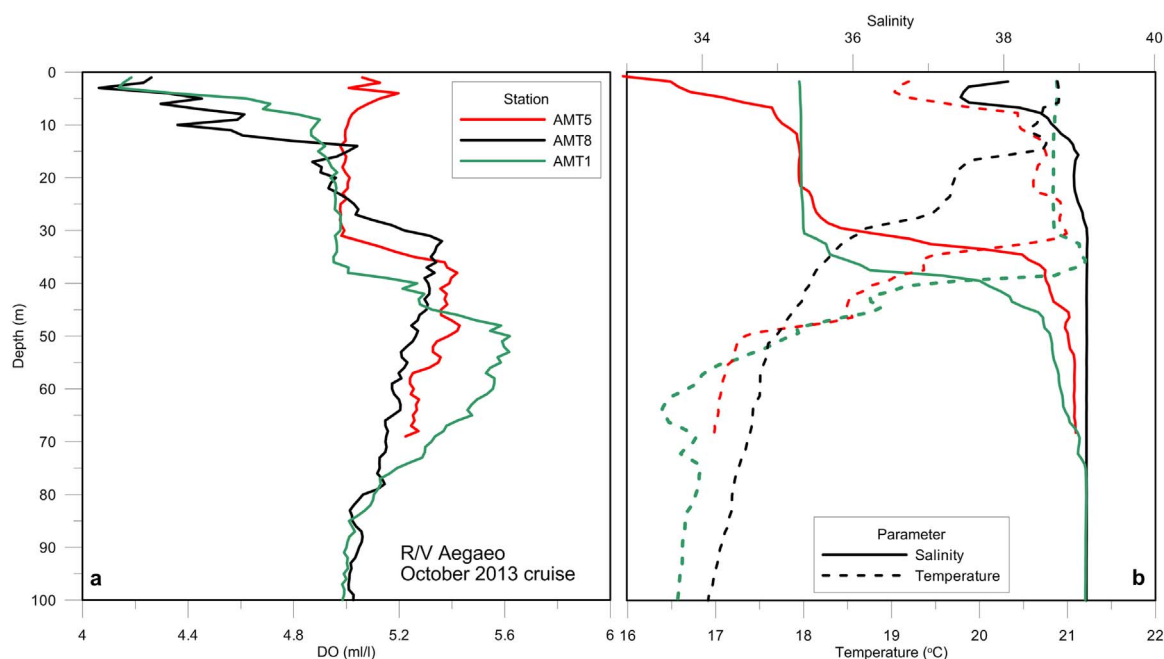


Fig. 18. Vertical profiles of (a) Dissolved Oxygen (ml/l) and (b) salinity (solid line) and temperature (dashed line), measured over the upper 100 m of AM1 (green), AM5 (red), and AM8 (black) stations (Fig. 1) by R/V Aegeao in October 2013 cruise. (For interpretation of the references to color in this figure legend, the reader is referred to the web version of this article).

than 50 m, reached the surface during the upwelling events of summer 2002. On the contrary, waters of Black Sea origin, with lower DO concentrations at the surface than the subsurface masses, may cover the Lesvos region and slightly increase the *AOU* levels during non-upwelling periods.

5. Conclusions

We used observations in tandem with numerical simulations to investigate and describe the major upwelling characteristics in the N. Aegean Sea and especially over the Lesvos coastal region (eastern Aegean coasts). The summer 2002 is a good example of many upwelling events in combination with periods of upwelling absence. Three periods of persistent northerly winds are detected, revealing five strong upwelling events and an in-between long period of upwelling unfavorable conditions during summer 2002. All upwelling events were related to strong northerly winds, which displaced surface waters offshore, following different circulation patterns. The initial movement of the colder waters during the first days after an upwelling event under the cyclonic circulation over the central region (Central Aegean Eddies) in combination with the Black Sea Waters (BSW) branches and the Aegean cyclonic circulation along the coasts determined the fate of the up-welled waters over the broader N. Aegean. The outflow of brackish waters through the Dardanelles under northerly winds may form the SW Branch, south of Limnos, and play an important role on the westward transport of the up-welled waters, towards the western Aegean coasts or/and towards the Chalkidiki Peninsula and over the deep N. Aegean basins.

Southerly winds on the other hand may diverge waters with low salinity, due to the mixing with the buoyant Black Sea Waters, away from the general Aegean cyclonic circulation along the western coasts and move them towards the central region and over Lesvos broader western area. The appearance of a buoyant barrier layer over the surface in combination with upwelling unfavorable southerly winds may weaken and even block the upwelling processes over the eastern Aegean region. Stratification was strong during these non-upwelling conditions and significantly low salinity waters dominated over the upper-ocean. The blocking effect of the westward Ekman transport due to the eastward intrusion of broader open sea waters towards the

coastal region in combination with the formation of the low salinity barrier layer may suppress any upwelling processes that would occur even if upwelling favorable conditions prevail (northerly winds). The attenuation or the absence of northerly winds weaken and even eliminate upwelling over the coastal region, increasing the surface temperature and strengthening the stratification of the upper-ocean. Large upwelling depths usually lead to the arrival of colder, richer and denser waters over the sea surface. However, the upwelling depth over the Lesvos coastal region is not deep, restricted within the subsurface ocean (< 40 m). Stratification is weak during upwelling periods, especially at depths, where upwelling processes are intense ($N \rightarrow 0$), allowing dense waters to mix and emerge towards the upper layers.

Oxygen-depleted waters are usually transferred towards the surface from deeper anoxic layers during upwelling conditions and stronger upwelling usually results in lower DO over the shallow coastal waters (Roegner et al., 2011). However, in the case of N. Aegean upwelling, waters depleted from nutrients with higher DO concentrations are transferred to the surface due to the shallow upwelling depth (15–40 m) from within the thermocline over the Lesvos coastal region, as presented during the five study events. The upwelling waters are originated from the subsurface N. Aegean layers, characterized by lower Apparent Oxygen Utilization (*AOU*) values than the surface pre-existing masses, which are influenced by the BSW plume (low salinity levels), especially during non-upwelling periods. However, the fact that these upwelling events took place mostly during the summer stratified season when the surface layers are depleted from nutrients, and the upwelling waters come from above the thermocline nutrient depleted layer, is an indicator that no major blooming events can be triggered in the central and eastern Aegean after upwelling events.

Due to the shallow upwelling depth, the acceleration of the warming rate in the Aegean Sea during the last two decades (Skirris et al., 2011) may have a strong counter effect on the development of upwelling processes along the eastern coasts. Moreover, Nykjaer (2009) showed that the heat accumulation in the upper layers of the Aegean Sea occurred mainly during August, when usually Etesian winds prevail and upwelling events occur. These effects remain to be investigated through subsequent work. The L1 Poseidon Buoy's location over the western Lesvos region is unique to measure and detect upwelling summer events. Additionally, the use of NAS-HYCOM, which was

previously used to investigate several Aegean features such as the BSW circulation patterns (Androulidakis and Kourafalou, 2011), the dense water formation processes (Androulidakis et al., 2012a) and the connectivity between Aegean and Black Sea through the Dardanelles (Androulidakis et al., 2012b), supported the findings derived from the measurements and investigated the broader implications of both BSW and up-welled waters.

Acknowledgments

This research was conducted in the framework of the AegeanMarTech project: The AegeanMarTech project - “Technological and oceanographic cooperation Network for the Study of mechanisms fertilizing the North-East Aegean Sea” (Project code nr/MIS:383548) was implemented through the Operational Program “Education and Lifelong Learning 2007–2013” (CCI:2007GRO5UPO002) of the National Strategic Reference Framework (NSRF), more specifically through the Research Funding Program: “THALES” and has been co-financed by the European Union (European Social Fund) and Greek National Funds. We are grateful to Alan Wallcraft (Naval Research Laboratory) for providing the MED-HYCOM fields and Gerassimos Korres (Hellenic Centre of Marine Research; HCMR) for providing the atmospheric forcing fields from the Poseidon Forecasting System. The ocean observational data were provided by the HCMR's Poseidon Buoy System and the 2013 October cruise conducted by R/V Aegean in the framework of the THALES project. The GHRSSST data were obtained through the online PO.DAAC Live Access Server (LAS) at the Physical Oceanography Distributed Active Archive Center (PO.DAAC), NASA Jet Propulsion Laboratory. The chl-a satellite fields were obtained through the online Copernicus Marine Environment Monitoring Service.

References

- Albanakis, C., 1999. Oceanography Lectures. University Studio Press, Thessaloniki, 160, (in Greek).
- Androulidakis, Y.S., Kourafalou, V.H., 2011. Evolution of a buoyant outflow in the presence of complex topography: the Dardanelles plume (North Aegean Sea). *J. Geophys. Res.: Oceans* (1978–2012) 116 (C4).
- Androulidakis, Y.S., Krestenitis, Y.N., Kourafalou, V.H., 2012b. Connectivity of North Aegean circulation to the Black Sea water budget. *Cont. Shelf Res.* 48, 8–26.
- Androulidakis, Y.S., Kourafalou, V.H., Krestenitis, Y.N., Zervakis, V., 2012a. Variability of deep water mass characteristics in the North Aegean Sea: the role of lateral inputs and atmospheric conditions. *Deep Sea Res. Part I: Oceanogr. Res. Pap.* 67, 55–72.
- Bleck, R., 2002. An oceanic general circulation model framed in hybrid isopycnic-cartesian coordinates. *Ocean Model.* 4 (1), 55–88.
- Cabrera, O.C., Villanoy, C.L., David, L.T., Gordon, A.L., 2011. Barrier layer control of entrainment and upwelling in the Bohol Sea, Philippines. *Oceanography* 24 (1), 130–141.
- Chassignet, E.P., Hurlburt, H.E., Smedstad, O.M., Halliwell, G.R., Hogan, P.J., Wallcraft, A.J., Baraille, R., Bleck, R., 2007. The HYCOM (hybrid coordinate ocean model) data assimilating system. *J. Mar. Syst.* 65 (1), 60–83.
- Donlon, C.J., Casey, K.S., Robinson, I.S., Gentemann, C.L., Reynolds, R.W., Barton, I., Arino, O., Stark, J., Rayner, N., Le Borgne, P., Poulter, D., 2009. The GODAE high resolution sea surface temperature pilot project. *Oceanography* 22 (3), 34–45.
- Garcia, H.E., Gordon, L.I., 1992. Oxygen solubility in seawater: Better fitting equations. *Limnol. oceanogr.* 37 (6), 1307–1312.
- Garcia, H.E., Boyer, T.P., Levitus, S., Locarnini, R.A., Antonov, J., 2005. On the variability of dissolved oxygen and apparent oxygen utilization content for the upper world ocean: 1955 to 1998. *Geophys. Res. Lett.* 32 (9).
- Garraffo, Z.D., Mariano, A.J., Griffa, A., Veneziani, C., Chassignet, E.P., 2001. Lagrangian data in a high-resolution numerical simulation of the North Atlantic: I. Comparison with in situ drifter data. *J. Mar. Syst.* 29 (1), 157–176.
- Gopinath, A., Sindhu, R., Nair, S.M., 2006. Variability of dissolved reactive phosphate and apparent oxygen utilization along the west coast of India. *Chem. Ecol.* 22 (2), 113–123.
- Halliwell, G.R., 2004. Evaluation of vertical coordinate and vertical mixing algorithms in the HYbrid-Coordinate Ocean Model (HYCOM). *Ocean Model.* 7 (3), 285–322.
- Ignatiades, L., Psarra, S., Zervakis, V., Pagou, K., Souvermezoglou, E., Assimakopoulou, G., Gotsis-Skretas, O., 2002. Phytoplankton size-based dynamics in the Aegean Sea (Eastern Mediterranean). *J. Mar. Syst.* 36 (1), 11–28.
- Kallos, G., Nickovic, S., Papadopoulos, A., Jovic, D., Kakaliagou, O., Misirlis, N., Boukas, L., Mimikou, N.G.S.J.P., Sakellaridis, G., Papageorgiou, J., Anadranistakis, E., 1997. The regional weather forecasting system SKIRON: an overview. In: Proceedings of the Symposium on Regional Weather Prediction on Parallel Computer Environments, Vol. 15, p. 17.
- Kourafalou, V.H., Barbopoulos, K., 2003. High resolution simulations on the North Aegean Sea seasonal circulation. *Ann. Geophys.* 21 (1), 251–265.
- Kucuksezgin, F., Balci, A., Kontas, A., Altay, O., 1995. Distribution of nutrients and chlorophyll-a in the Aegean sea. *Oceanol. Acta* 18 (3), 343–352.
- Lagaria, A., Mandalakis, M., Mara, P., Frangoulis, C., Karatsolis, B.-Th., Pitta, P., Triantaphyllou, M., Tsiola, A., Psarra, S., 2016. Phytoplankton variability and community structure in relation to hydrographic features in the NE Aegean frontal area (NE Mediterranean Sea). *Cont. Shelf Res.* <http://dx.doi.org/10.1016/j.csr.2016.07.014>.
- Lykousis, V., Chronis, G., Tselepidis, A., Price, N.B., Theocharis, A., Siokou-Frangou, I., Van Wambeke, F., Danovaro, R., Stavrakakis, S., Duineveld, G., Georgopoulos, D., 2002. Major outputs of the recent multidisciplinary biogeochemical researches undertaken in the Aegean Sea. *J. Mar. Syst.* 33, 313–334.
- Maderich, V., Ilyin, Y., Lemesko, E., 2015. Seasonal and interannual variability of the water exchange in the Turkish Straits System estimated by modelling. *Mediterr. Mar. Sci.* <http://dx.doi.org/10.12681/mms.1103>.
- Millan-Nunez, R., Alvarez-Borrego, S., Nelson, D.M., 1982. Effects of physical phenomena on the distribution of nutrients and phytoplankton productivity in a coastal lagoon. *Estuar. Coast. Shelf Sci.* 15 (3), 317–335.
- Nittis, K., Perivoliotis, L., 2002. Circulation and hydrological characteristics of the North Aegean Sea: a contribution from real-time buoy measurements. *Mediterr. Mar. Sci.* 3 (1), 21–32.
- Nittis, K., Zervakis, V., Papageorgiou, E., Perivoliotis, L., 2002. Atmospheric and oceanic observations from the POSEIDON buoy network: initial results. *Glob. Atmos. Ocean Syst.* 8 (2–3), 137–149.
- Nykjaer, L., 2009. Mediterranean Sea surface warming 1985–2006. *Clim. Res.* 39 (1), 11–17.
- Olson, D.B., Kourafalou, V.H., Johns, W.E., Samuels, G., Veneziani, M., 2007. Aegean surface circulation from a satellite-tracked drifter array. *J. Phys. Oceanogr.* 37 (7), 1898–1917.
- Papadopoulos, A., Katsafados, P., Kallos, G., Nickovic, S., 2002. The weather forecasting system for POSEIDON-An overview. *Glob. Atmos. Ocean Syst.* 8 (2–3), 219–237.
- Pazi, I., 2008. Water mass properties and chemical characteristics in the Saros Gulf, northeast Aegean Sea (Eastern Mediterranean). *J. Mar. Syst.* 74 (1), 698–710.
- Pearson, K., 1903. Mathematical contributions to the theory of evolution. XI. On the influence of natural selection on the variability and correlation of organs. *Philos. Trans. R. Soc. Lond. Ser. A Contain. Pap. A Math. Phys. Character.* 1–66.
- Poulos, S.E., Drakopoulos, P.G., Collins, M.B., 1997. Seasonal variability in sea surface oceanographic conditions in the Aegean sea (Eastern Mediterranean): an overview. *J. Mar. Syst.* 13 (1), 225–244.
- Qu, T., Meyers, G., 2005. Seasonal variation of barrier layer in the southeastern tropical Indian Ocean. *J. Geophys. Res.: Oceans* 110 (C11).
- Roegner, G.C., Needoba, J.A., Baptista, A.M., 2011. Coastal upwelling supplies oxygen-depleted water to the Columbia River estuary. *PLoS One* 6 (4), e18672.
- Savvidis, Y.G., Dodou, M.G., Krestenitis, Y.N., Koutitas, C.G., 2004. Modeling of the upwelling hydrodynamics in the Aegean Sea. *Mediterr. Mar. Sci.* 5, 5–18.
- Sayin, E., Eronat, C., Uçkaç, Ş., Beşiktepe, Ş.T., 2011. Hydrography of the eastern part of the Aegean Sea during the Eastern Mediterranean Transient (EMT). *J. Mar. Syst.* 88 (4), 502–515.
- Siokou-Frangou, I., Zervoudaki, S., Christou, E.D., Zervakis, V., Georgopoulos, D., 2009. Variability of mesozooplankton spatial distribution in the North Aegean Sea, as influenced by the Black Sea waters outflow. *J. Mar. Syst.* 78 (4), 557–575.
- Siokou-Frangou, I., Bianchi, M., Christaki, U., Christou, E.D., Giannakourou, A., Gotsis, O., Ignatiades, L., Pagou, K., Pitta, P., Psarra, S., Souvermezoglou, E., 2002. Carbon flow in the planktonic food web along a gradient of oligotrophy in the Aegean Sea (Mediterranean Sea). *J. Mar. Syst.* 33, 335–353.
- Skliris, N., Mantziafou, A., Sofianos, S., Gkanasos, A., 2010. Satellite-derived variability of the Aegean Sea ecohydrodynamics. *Cont. Shelf Res.* 30 (5), 403–418.
- Skliris, N., Sofianos, S.S., Gkanasos, A., Axaopoulos, P., Mantziafou, A., Vervatis, V., 2011. Long-term sea surface temperature variability in the Aegean sea. *Adv. Oceanogr. Limnol.* 2 (2), 125–139.
- Souvermezoglou, A., Krasakopoulou, E., Pavlidou, A., 2014. Temporal and spatial variability of nutrients and oxygen in the North Aegean Sea during the last thirty years. *Mediterr. Mar. Sci.* 15 (4), 805–822.
- Steel, R.G., James, H., 1960. Principles and Procedures of Statistics: with Special Reference to the Biological Sciences (No. 519.5 S314p). McGraw-Hill, New York, US.
- Theocharis, A., Nittis, K., Kontoyiannis, H., Papageorgiou, E., Balopoulos, E., 1999. Climatic changes in the Aegean Sea influence the eastern Mediterranean thermohaline circulation (1986–1997). *Geophys. Res. Lett.* 26 (11), 1617–1620.
- Tsiaras, K.P., Petihakis, G., Kourafalou, V.H., Triantafyllou, G., 2014. Impact of the river nutrient load variability on the North Aegean ecosystem functioning over the last decades. *J. Sea Res.* 86, 97–109.
- Tsiaras, K.P., Kourafalou, V.H., Raitos, D.E., Triantafyllou, G., Petihakis, G., Korres, G., 2012. Inter-annual productivity variability in the North Aegean Sea: influence of thermohaline circulation during the Eastern Mediterranean Transient. *J. Mar. Syst.* 96, 72–81.
- Turner, J.S., 1973. Buoyancy Effects in Fluids. Cambridge University Press, New York, 367.
- Ünlüata, Ü., 1986. A Review of the Physical Oceanography of the Levantine and the Aegean Basins of the Eastern Mediterranean in Relation to Monitoring and Control of Pollution. Institute of Marine Sciences, Middle East Technical University.
- Ünlüata, Ü., Oğuz, T., Latif, M.A., Özsoy, E., 1990. On the physical oceanography of the Turkish Straits. The physical oceanography of sea straits. *Kluwer Acad. Publ.*, 25–60.
- Valioulis, I.A., Krestenitis, Y.N., 1994. Modelling the water mass circulation in the Aegean Sea. Part I: wind stresses, thermal and haline fluxes. In: *Annales Geophysicae*, Springer-Verlag, Vol. 12, No. 8, pp. 794–807.

- Willmott, C.J., 1981. On the validation of models. *Phys. Geogr.* 2 (2), 184–194.
- Xie, J., Zhu, J., Li, Y., 2008. Assessment and inter-comparison of five high-resolution sea surface temperature products in the shelf and coastal seas around China. *Cont. Shelf Res.* 28 (10), 1286–1293.
- Yüce, H., 1995. Northern Aegean water masses. *Estuar. Coast. Shelf Sci.* 41 (3), 325–343.
- Zeri, C., Beşiktepe, Ş., Giannakourou, A., Krasakopoulou, E., Tzortziou, M., Tsoliakos, D., Pavlidou, A., Mousdis, G., Pitta, E., Scoullou, M., Papathanassiou, E., 2014. Chemical properties and fluorescence of DOM in relation to biodegradation in the interconnected Marmara–North Aegean Seas during August 2008. *J. Mar. Syst.* 135, 124–136.
- Zervakis, V., Georgopoulos, D., 2002. Hydrology and circulation in the North Aegean (eastern Mediterranean) throughout 1997 and 1998. *Mediterr. Mar. Sci.* 3 (1), 5–19.
- Zervakis, V., Georgopoulos, D., Drakopoulos, P.G., 2000. The role of the North Aegean in triggering the recent eastern Mediterranean climatic changes. *J. Geophys. Res.* 105 (C11), 26103–26116.
- Zervoudaki, S., Kaliva, K., Apostolopoulou-Moraitou, M., 1999. Seasonal variation of hydrobiochemical variables in a coastal area of an ichthyoculture. In: *Proceedings of the 6 th International Conference on Environmental Science and Technology*, Vol. 100, pp. 474–481.
- Zodiatis, G., 1994. Advection of the Black Sea water in the north Aegean Sea. *Glob. Atmos. Ocean Syst.* 2 (1), 41–59.